ORNL/TM-2024/3437

Summary of Leach-Burn-Leach Round-Robin Test Results

John D. Hunn

June 2024

Approved for public release.
Distribution is unlimited.

OAK RIDGE National Laboratory

ORNL IS MANAGED BY UT-BATTELLE LLC FOR THE US DEPARTMENT OF ENERGY

ORNL/TM-2024/3437

Nuclear Energy and Fuel Cycle Division

SUMMARY OF LEACH-BURN-LEACH ROUND-ROBIN TEST RESULTS

John D. Hunn

Revision 0

June 2024

Prepared by
OAK RIDGE NATIONAL LABORATORY
Oak Ridge, TN 37831
managed by
UT-BATTELLE, LLC
for the
US DEPARTMENT OF ENERGY
under contract DE-AC05-00OR22725

CONTENTS

LIST OF FIGURES

LIST OF TABLES

ABBREVIATIONS

BL	burn-leach
DUO_2	depleted uranium dioxide (kernels)
FB-CVD	fluidized-bed chemical vapor deposition
GIF	Generation IV International Forum
FIB	focused ion beam
HTGR	high-temperature gas-cooled reactor
ICP-MS	inductively coupled plasma mass spectrometry
ID	identity
INET	Institute of Nuclear and New Energy Technology
IPyC	inner pyrolytic carbon (TRISO layer)
KAERI	Korea Atomic Energy Research Institute
LBL	leach-burn-leach
MDL	minimum detection limit
NA	not applicable
NIST	National Institute of Standards and Technology
OPyC	outer pyrolytic carbon (TRISO layer)
ORNL	Oak Ridge National Laboratory
PE-U	particle equivalents of uranium
PIE	post-irradiation examination
ppm	parts per million
QC	quality control
SD	standard deviation
SiC	silicon carbide (TRISO layer)
SRM	Standard Reference Material
TRISO	tristructural-isotropic (coated particles)
UCO	mixture of uranium carbide and uranium oxide (kernels)
UO_2	uranium dioxide (kernels)
XCT	x-ray computed tomography
ZrO_2	zirconium dioxide (surrogate kernels)

ACKNOWLEDGMENTS

Preparation of the summary report was sponsored by the US Department of Energy Office of Nuclear Energy—Advanced Reactor Technologies under the Advanced Gas Reactor Fuel Development and Qualification Program. Special thanks go to Dr. Grant W. Helmreich for technical review of the probability discussion in Section 4.1 and assistance in preparing Figure 4-1 through Figure 4-3. Thanks also to Dr. Tyler J. Gerczak for review of this report and help in coordinating ORNL's part of the round-robin test.

1. BACKGROUND

1.1 INTRODUCTION

Tristructural isotropic (TRISO) coated particle fuel is of interest to multiple member states associated with the Generation IV International Forum (GIF). Qualification and acceptance testing of TRISO fuel includes the determination of particle defect fractions and impurities in the as-fabricated TRISO fuel particle and/or composited fuel form, which are typically determined using burn-leach (BL) or leach-burn-leach (LBL) analysis methods. A round-robin test focusing on LBL analysis was undertaken by the GIF Very High Temperature Reactor System Fuel and Fuel Cycle Project Management Board. Participating in this LBL round-robin test were research staff from the Institute of Nuclear and New Energy Technology (INET) in the People's Republic of China, the Korean Atomic Energy Research Institute (KAERI) in the Republic of Korea, and Oak Ridge National Laboratory (ORNL) in the United States of America. The motivation of this LBL benchmarking exercise was to explore consistency in results generated by LBL and to elucidate the potential influence of variations in the procedures used by the participating members on the accurate determination of the measured fuel properties.

The typical design for the TRISO-coated particles used in high-temperature gas-cooled reactors (HTGRs) consists of a ceramic fuel kernel, typically uranium dioxide (UO_2) or a mixture of uranium carbide and uranium oxide called *UCO*, encased in multiple layers deposited by fluidized-bed chemical vapor deposition (FB-CVD). A porous carbon buffer layer is deposited on the kernel to accommodate kernel swelling and fission product recoil. Surrounding this buffer layer are three isotropic layers—the inner pyrolytic carbon (IPyC), silicon carbide (SiC), and outer pyrolytic carbon (OPyC) layers—that provide structural stability and a diffusion barrier. For graphite-moderated HTGRs with a prismatic core or pebble-bed core, the TRISO particles are typically surrounded with a resinated graphite powder and formed under pressure into either cylindrical compacts or spherical pebbles, respectively. The pressed fuel forms are heated to carbonize the resin, leaving a graphitic matrix that encapsulates the particles.

Compromised coating layers in TRISO fuel particles, caused by flaws in the fabrication process, damage from handling, degrading reactions between the coating layers and metallic impurities, or coating failures cause by irradiation in a reactor, can affect the performance of the TRISO coating with respect to its ability to retain fission products as designed. Two types of compromised particles that can be detected and quantified by LBL to evaluate TRISO fuel quality are *exposed-kernel defects* (kernels not retained within at least one hermetic layer) and *SiC defects* (kernels not encased by a normally retentive SiC layer but with at least one hermetic pyrolytic carbon layer). Compromised SiC in conjunction with at least one normal pyrocarbon layer is typically less impactful than when the kernel is fully exposed because the hermetic seal afforded by the pyrocarbon maintains a more stable kernel chemistry such that many fission products will remain in the kernel.

In the LBL process, exposed-kernel defects are detected in the first phase of leaching (before the burn phase). In particles with fully compromised TRISO coatings, hot nitric acid contacts the exposed kernel and dissolves the uranium. Uranium measured in the preburn leach solutions can be converted to a particle-equivalent value by dividing the measured grams of uranium by the average grams of uranium in one kernel. Thus, the number of particles with exposed-kernel defects can be enumerated if leaching is effective. The burn phase of LBL is designed to remove all exposed carbon by oxidation at elevated temperature. This includes the removal of all OPyC layers, removal of carbon pathways through the SiC (such as may be caused by carbon soot inclusions during FB-CVD or by high-temperature chemical degradation of the SiC by metallic impurities that form silicides), and removal of the IPyC and buffer layers inside of TRISO particles with defective SiC. The postburn leach phase will dissolve uranium in particles with defective SiC whose kernels were exposed by an effective burn phase. Enumeration of particles with defective SiC is achieved by determining the total particle equivalents of uranium in the postburn leach solutions.

1.2 SAMPLES FOR LEACH-BURN-LEACH ROUND-ROBIN TEST*

The cooperative round-robin test included two types of samples for comparative LBL analysis. The two types were (1) representative sublots containing uranium-bearing TRISO particles produced in a production-size coater and (2) simulated samples containing ~10,000 surrogate (nonuranium-bearing) TRISO particles added to which were up to four uranium-bearing TRISO particles with simulated defects in addition to carbon powder containing a known amount of various relevant impurities (Gerczak et al. 2022). The series of simulated samples provided to each participant included examples of both types of defective particles relevant to LBL (exposed-kernel defects and SiC defects). Because the simulated samples had known numbers and types of defective particles and known masses of various impurities, they were useful in exploring the accuracy and consistency of the LBL methods employed by each participant. The analysis of the representative sublots provided a way to compare results obtained from analysis of multiple samples from the same coating batch that were representative of typical TRISO fuel.

The representative sublots consisted of TRISO particles with depleted uranium dioxide (DUO_2) kernels prepared by INET. Participants were to be provided four samples riffled from a single large parent lot so that measured results could be statistically compared. Three ~40 g representative TRISO samples were to be subjected to LBL analysis by each participant to measure defect fractions. One ~10 g sample was reserved for determining the average uranium loading per particle.

The simulated samples were supplied to each participant by ORNL. Details on the production of the particles with simulated defects can be found in ORNL/TM-2015/722, *Preparation of Simulated LBL Defects for Round-Robin Experiment* (Gerczak et al. 2022). Particles with simulated defects were produced using DUO_2 TRISO particles fabricated at ORNL in coating batch DUN500S-10A. The exposed-kernel defects were produced by subjecting fully TRISO-coated particles to a single-point impact, which resulted in fractures propagating through all the TRISO layers and exposing the kernel. These simulated defects represent a type of exposed-kernel defect that has been observed in TRISO fuel manufacturing and can be identified during the preburn leach phase of the LBL analysis. Each particle with a simulated exposed-kernel defect was verified with x-ray computed tomography (XCT) before it was added to a simulated sample used for the round-robin test. The XCT-generated cross section (tomogram) in Figure 1-1 shows a fracture that exposed the kernel in a particle with a simulated exposed-kernel defect. Particles with SiC defects were simulated using burned-back DUO_2 TRISO particles from batch DUN500S-10A. The burn-back was implemented to remove the OPyC layer because of limitations in the dimensions of the hole that could be produced with the method used to fabricate the simulated defects (Gerczak et al. 2022). A dual-beam focused ion beam (FIB), scanning electron microscope was used to locally mill a 25 μm diameter hole through the SiC layer, exposing the IPyC layer without penetrating it. Figure 1-2 shows an example of a simulated SiC defect produced in a particle for the LBL round-robin test. Each particle with a simulated SiC defect was verified with x-ray radiography before it was added to a simulated sample used for the round-robin test.

A series of seven individual simulated samples were supplied to each participant. Each contained ~10,000 surrogate coated particles with ~500 μm diameter zirconium dioxide (ZrO_2) kernels and a known quantity of an impurity standard, namely National Institute of Standards and Technology (NIST) Standard Reference Material (SRM) 1632d, which contained relevant concentrations of many of the elements of interest to fuel performance and/or post-irradiation examination (PIE). One of the seven samples in each series contained no particles with simulated defects; this sample served as a baseline. Three samples contained either one, two, or four particles with simulated exposed-kernel defects. The other three samples contained either one, two, or four particles with simulated SiC defects. The samples were labeled with the acronym for the participating research institution and an alphabetical sequence (e.g., ORNL-A

* This section was copied from ORNL/TM-2023/2951 (Hunn et al. 2023) and is included herein, with a few editorial modifications, for context and terminology.

through ORNL-G). The number of simulated defects in each sample was not shared with the participants so as to maintain a blind study. Requested reporting included the amounts of uranium and relevant impurities measured in each leach phase, as well as the number and type of defect in each simulated sample. After each institution had completed and reported on LBL analysis of their simulated sample set at a GIF meeting, information on the population of particles with simulated defects and the masses of the added impurities was distributed to participants via a revision to ORNL/TM-2015/722 (Gerczak et al. 2022) for use in individual reporting. Appendix A contains this information for simulated samples ORNL-A through ORNL-G, INET-A through INET-G, and KAERI-A through KAERI-G.

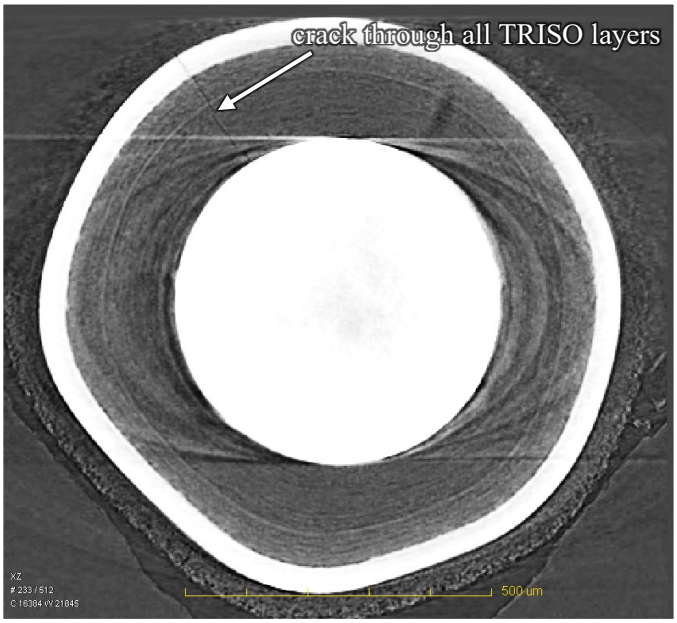

Figure 1-1. XCT tomogram of a DUN500S-10A particle with a simulated exposed-kernel defect that was produced by single-point impact. Image from Gerczak et al. (2022).

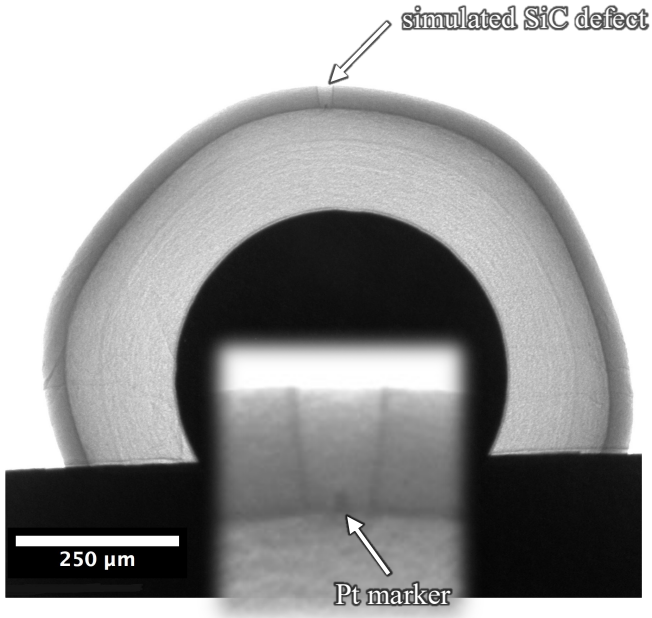

Figure 1-2. X-ray radiograph showing a simulated SiC defect that terminates near the IPyC–SiC interface. Inset shows a close-up of the simulated defect with a platinum marker to mark the bottom of the milled feature. Images from Gerczak et al. (2022).

2. COMPARISON OF LEACH-BURN-LEACH PROCEDURES

Individual reports were produced by each participant that discuss the results of their analyses and describe the unique LBL procedures they used (Xu and Chen 2023; Yeo 2024; Hunn et al. 2023). Table 2-1 summarizes the parameters used for LBL by each round-robin participant. Several notable differences exist, and the impact of these differences is considered in the discussion of the results of the LBL analyses of the simulated samples in Section 4.

Table 2-1. Comparison of LBL Procedures Used by INET, KAERI, and ORNL

LBL Stage	Parameter	INET	KAERI	ORNL
Preburn Leach	Nitric acid concentration (wt%)	34–35	60	68–70
	Nitric acid temperature (°C)	98	90	~120
	Leach time (h)	2	48	24 (twice)
Burn	Furnace temperature (°C)	850	800	750
	Burn time (h)	16	10	72
Postburn Leach	Nitric acid concentration (wt%)	34–35	60	68–70
	Nitric acid temperature (°C)	98	90	~120
	Leach time (h)	8	48	24 (twice)

The process employed at INET involved significantly lower acid concentration and shorter leaching times. Total leaching times at KAERI and ORNL were the same, but two sequential leaches were performed at ORNL for both preburn and postburn leaching to provide feedback on whether leaching was complete (Hunn et al. 2023), whereas one longer leach for each stage was completed at KAERI. Acid temperature during leaching at ORNL was higher, as the 68%–70% concentration of nitric acid was held at or near its boiling point. At 68% concentration, nitric acid forms an azeotrope with water, such that concentration does not change with boiling. At lower concentrations, nitric acid can be concentrated when heating due to relatively higher loss of water below the azeotropic concentration. However, water-cooled condensers were used by all participants, which maintained the leachate volumes during heating and minimized concentration increases in the non-azeotropic solutions.

For an effective burn phase, a sufficient combination of time and temperature is needed to remove the OPyC and also to allow oxygen to penetrate through a compromised SiC layer and fully oxidize the IPyC, buffer, and, preferably, the kernel as well to increase its overall solubility. All participants used furnace temperatures sufficient to oxidize exposed pyrocarbon. The temperature used at ORNL was the lowest of the participants but was offset by a longer burn time.

Inductively coupled plasma mass spectrometry (ICP-MS) was used at ORNL to measure both uranium and the metallic impurities of interest. Laser fluorescence spectrometry was used at INET for uranium, whereas ICP-MS was used for measurement of metallic impurities. The KAERI report lists the use of inductively coupled plasma optical emission spectrometry (ICP-OES) in addition to ICP-MS.

3. COMPARISON OF ANALYSIS RESULTS FOR REPRESENTATIVE SUBLOTS

Four samples containing TRISO-coated DUO_2 kernels were sent from INET to ORNL. These samples were representative of particles produced by a production-scale coater and were randomly riffled sublots from a single coating batch. The three 40 g representative sublots sent to ORNL were subjected to LBL, and leachates were analyzed for uranium content and metallic impurities. Detailed results of this analysis are discussed in the ORNL report (Hunn et al. 2023). Uranium content was also measured in three 25 g representative sublots at INET, and results of that analysis are provided in the INET report (Xu and Chen 2023). Impurity analysis on the representative samples was not performed at INET because the INET quality control (QC) system mostly focuses on impurity content in the graphite matrix. However, impurity analysis at ORNL showed relatively low content for the metallic impurities normally targeted during QC inspection, so better comparisons for impurity analysis are available from the simulated samples discussed in Section 4. Representative sublots were not available for analysis at KAERI due to issues with obtaining approval for international exchange of uranium-bearing materials.

Table 3-1 shows the amount of uranium detected during preburn and postburn leaching of the 40 g representative sublots sent to ORNL and the three 25 g representative sublots measured at INET. Values are given in parts per million (ppm) by weight (uranium mass / sublot mass) and in terms of the particle equivalent of uranium. None of the sublots subjected to LBL at ORNL or INET contained particles with either SiC or exposed-kernel defects, as attested by the low uranium content in the leachates. When uranium is detected in the LBL leachates at a level well below one particle equivalent, it is often interpreted as general uranium contamination not associated with defective or failed particles. Such contamination can come from pickup in the processing equipment, such as the FB-CVD furnace, whose internals are exposed to bare kernels at the beginning of the coating process. Although the samples measured by ORNL and INET were randomly acquired from the same batch and contained roughly 18,000–31,000 particles each, the measured uranium content varied. Some of this variation may have been associated with the uncertainty in measuring such relatively low concentrations. However, Sample O-3 in Table 3-1 appeared to have a significantly higher uranium content that could have come from discrete uranium contamination localized to a single particle in that sublot (Hunn et al. 2023).

Table 3-1. Comparison of U Contamination Measured by LBL at INET and ORNL

Leach stage	Uranium content	INET			ORNL		
		I-1	I-2	I-3	O-1	O-2	O-3
Preburn	ppm by weight	0.0459	0.0447	0.0332	0.00623	0.00646	0.14504
	particle equivalents	0.00192	0.00187	0.00139	0.00044	0.00045	0.00943
Postburn	ppm by weight	0.0386	0.0163	0.0169	0.02219	0.00625	0.00501
	particle equivalents	0.00161	0.00068	0.00071	0.00155	0.00043	0.00033
Total	ppm by weight	0.0845	0.0610	0.0501	0.02842	0.01271	0.15006
	particle equivalents	0.00353	0.00255	0.00209	0.00199	0.00088	0.00976

Also discussed in the ORNL report are the results from the measurement of the average uranium loading in three subsamples riffled from the 10 g representative sublot sent to ORNL. The procedure for uranium loading at ORNL involves burning off the OPyC, pulverizing the coating layers to expose all the kernels, burning the debris to remove the buffer and IPyC fragments and oxidize the kernels, and then dissolving the kernels in nitric acid. This procedure allows for dissolution of essentially all the uranium in the analyzed specimen. At the completion of the burn-crush-burn-leach process, uranium concentration is measured by Davies–Gray titration. The average uranium per particle measured at ORNL was 5.984E-4 g U per particle, with a standard deviation of 9.4E-7 g U per particle for the three subsamples that were analyzed (Hunn et al. 2023). This result compared well with an average uranium per particle measured at INET of 5.996E-4 g U (Xu and Chen 2023).

4. COMPARISON OF ANALYSIS RESULTS FOR SIMULATED SAMPLES

All round-robin participants received and performed LBL analysis on seven simulated samples containing ~10,000 surrogate (nonuranium-bearing) coated particles to which were added up to four uranium-bearing particles with simulated exposed-kernel defects or SiC defects, as well as carbon powder containing a known amount of various metallic impurities. Details on these samples are available in the sample preparation report (Gerczak et al. 2022), and tables describing the contents of each are in Appendix A. The simulated samples provided a round-robin test for the accuracy of each round-robin participant's LBL procedure for evaluating the presence of exposed-kernel defects or SiC defects and quantifying impurity content. Individual reports were produced by each participant that discuss the results of their analyses and describe the LBL procedures used (Xu and Chen 2023; Yeo 2024; Hunn et al. 2023). These results are compared in Sections 4.1 and 4.2, and the possible impact of variations in the LBL procedures are discussed.

4.1 URANIUM ANALYSIS BY LEACH-BURN-LEACH FOR DEFECT DETECTION

As discussed in Section 1.1, uranium measured in the preburn or postburn leachates is used as an indicator for the presence of exposed-kernel defects or SiC defects, respectively. Results obtained by each round-robin participant are shown in Table 4-1, in which the individual simulated sample IDs, A–G, are sorted according to the number and type of defects they contained per the information in Appendix A. The total mass of uranium leached from each simulated sample during the preburn and postburn leach stages are reported separately and as a combined total. In addition, Table 4-1 includes the results in terms of particle equivalents of uranium (PE-U), which were calculated by dividing the measured g U values by the average uranium per defective particle of 7.003E-4 g U (Gerczak et al. 2022).

Table 4-1. Comparison of U in Simulated Samples Measured by LBL at INET, KAERI, and ORNL

Defect number and type	Leach stage	INET			KAERI [a]			ORNL		
		ID	g U	PE-U	ID	g U	PE-U	ID	g U	PE-U
zero defects	preburn leach		1.00E-09	0.0000					2.93E-07	0.0004
	postburn leach	D	3.07E-06	0.0044	G			B	1.29E-07	0.0002
	combined		3.07E-06	0.0044					4.22E-07	0.0006
one exposed-kernel defect	preburn leach		3.07E-04	0.4379		6.40E-04	0.9139		6.56E-04	0.9372
	postburn leach	E	3.01E-04	0.4297	B	6.30E-06	0.0090	C	3.21E-08	0.0000
	combined		6.07E-04	0.8676		6.46E-04	0.9229		6.56E-04	0.9372
two exposed-kernel defects	preburn leach		5.95E-04	0.8504		1.40E-03	1.9991		1.25E-03	1.7872
	postburn leach	A	9.34E-04	1.3344	A	7.80E-06	0.0111	A	2.05E-07	0.0003
	combined		1.53E-03	2.1849		1.41E-03	2.0103		1.25E-03	1.7875
four exposed-kernel defects	preburn leach		1.28E-03	1.8306		2.90E-03	4.1411		2.79E-03	3.9866
	postburn leach	F	1.35E-03	1.9349	D			F	3.93E-07	0.0006
	combined		2.64E-03	3.7654		2.90E-03	4.1411		2.79E-03	3.9871
one SiC defect	preburn leach		1.00E-09	0.0000					4.88E-06	0.0070
	postburn leach	G	1.07E-03	1.5217	C	6.60E-04	0.9425	E	6.36E-04	0.9086
	combined		1.07E-03	1.5217		6.60E-04	0.9425		6.41E-04	0.9156
two SiC defects	preburn leach		1.00E-09	0.0000					3.82E-07	0.0005
	postburn leach	C	1.52E-03	2.1783	F	1.10E-03	1.5708	D	9.77E-04	1.3953
	combined		1.52E-03	2.1783		1.10E-03	1.5708		9.77E-04	1.3958
four SiC defects	preburn leach		1.00E-09	0.0000					7.22E-06	0.0103
	postburn leach	B	3.16E-03	4.5186	E	2.90E-03	4.1411	G	2.59E-03	3.6992
	combined		3.16E-03	4.5186		2.90E-03	4.1411		2.60E-03	3.7095

Note: Data highlighted red were outside the 99.7% probability interval, and data highlighted orange were outside the 95% probability interval but within the 99.7% probability interval (see Table 4-2).

[a] Gaps in the data for the KAERI analyses indicate that values were less than the reported minimum measurable value of 0.02 µg/mL, which equates to 2E-6 g U in the reported leachate volume of 100 mL (Yeo 2024).

In the LBL process, PE-U values are calculated as an indication of the number of particles of each defect type contained in a sample of particles. Individual TRISO particles in any given batch vary in uranium content due to normal production variability in kernel volume, density, and chemistry. Therefore, regardless of the effectiveness of uranium leaching and the experimental uncertainty in the analysis of uranium in the leachates, PE-U values associated with defective particles are not expected to be exact whole numbers. However, these PE-U values should be within a reasonable statistical variation of the actual number of defective particles if the LBL process is sufficient to access and dissolve the uranium in the defective particles. The distribution in the individual g U per particle was not directly determined for the DUN500S-10A particle batch used to make the simulated defects. However, a standard deviation of roughly 7% for the distribution in the individual g U per particle was estimated from the average measured kernel diameter of 516 µm and standard deviation in the measured diameter of 12 µm by approximating the kernel shape as spherical (Gerczak et al. 2022; Hunn 2004). Assuming the particles with simulated defects were randomly selected from a normally distributed batch with an average of 7.003E-4 g U per particle and a standard deviation of 7%, the probability intervals shown in Table 4-2 were calculated for LBL round-robin simulated samples containing one, two, or four defective particles. The probability intervals in Table 4-2 correspond to probabilities of 68% (one sigma level), 95% (two sigma level), or 99.7% (three sigma level) that the total uranium in a one, two, or four particle set was within the associated interval.

Table 4-2. Probabilities for Various Ranges of U Inventory in the Particles with Simulated Defects

Number of defects	Probability	g U	PE-U
one	68%	6.51E-04 – 7.49E-04	0.93 – 1.07
two	68%	1.33E-03 – 1.47E-03	1.90 – 2.10
four	68%	2.70E-03 – 2.90E-03	3.86 – 4.14
one	95%	6.02E-04 – 7.98E-04	0.86 – 1.14
two	95%	1.26E-03 – 1.54E-03	1.80 – 2.20
four	95%	2.61E-03 – 3.00E-03	3.72 – 4.28
one	99.7%	5.53E-04 – 8.47E-04	0.79 – 1.21
two	99.7%	1.19E-03 – 1.61E-03	1.70 – 2.30
four	99.7%	2.51E-03 – 3.10E-03	3.58 – 4.42

Most of the combined LBL results in Table 4-1 lie within their relevant 95% probability interval, which indicates that the amount of deviation in those measured results from a whole number value of PE-U could be related to an actual variability in the uranium content in each defective particle in the sample. In addition, most of the deviation in those measured results from the most likely mean values were within the expected ±10% uncertainty in the uranium analysis. Results outside the 95% and/or 99.7% probability intervals are highlighted in Table 4-1. There is a very low probability that the values outside the 99.7% probability intervals (highlighted in red in Table 4-1) represent the true total uranium content in the particles with simulated defects for those samples because that would require a highly unlikely selection of particles with outlying uranium content from the parent batch. It is reasonable to presume that the results highlighted in red in Table 4-1 include some inherent error, as discussed below. Those values that lie within the relevant 99.7% probability interval but outside the corresponding 95% probability interval (highlighted in orange in Table 4-1) also have a low probability of being accurate; however, given that 18 simulated samples were tested, one or possibly two samples close to the 95% probability boundaries are expected. The relative probability that the experimental results in Table 4-1 are reasonable with respect to the expected normal distribution for PE-U in the simulated samples is presented graphically in Figure 4-1 through Figure 4-3, in which the measured values for PE-U in each simulated sample are overlaid on the normal distribution for one, two, or four particles randomly selected from a particle source with an average of 7.003E-4 g U per particle and a standard deviation of 7%, respectively.

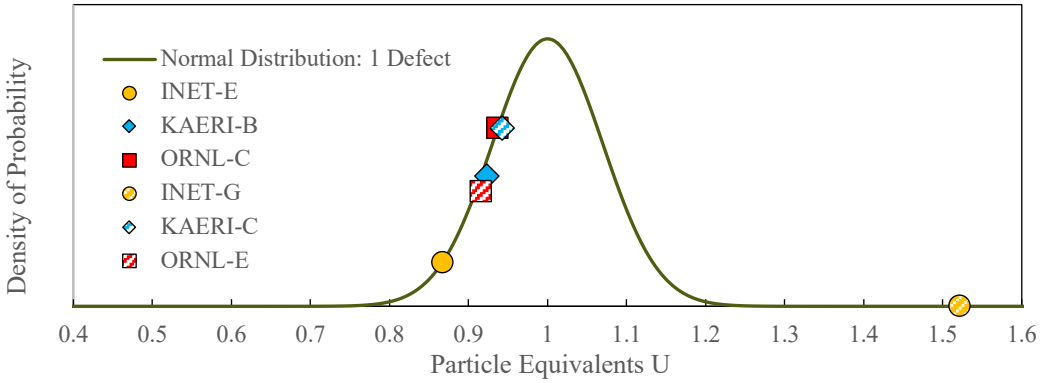

Figure 4-1. Normal distribution for uranium simulated samples with one defect versus measured values.

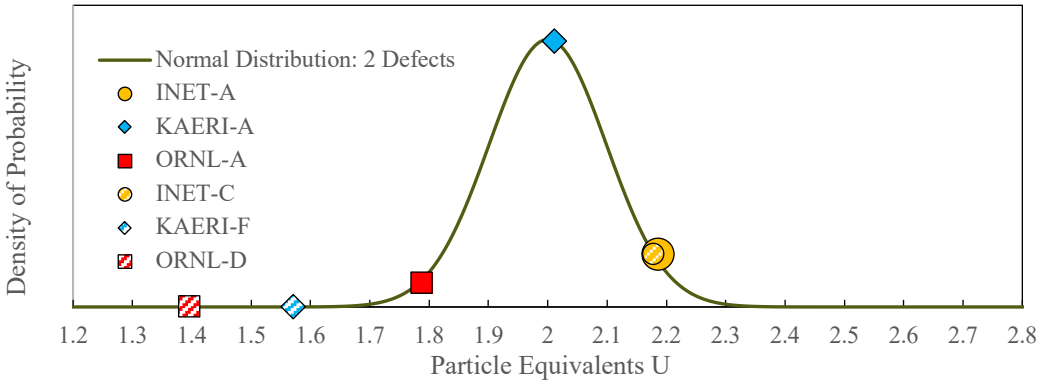

Figure 4-2. Normal distribution for uranium simulated samples with two defects versus measured values.

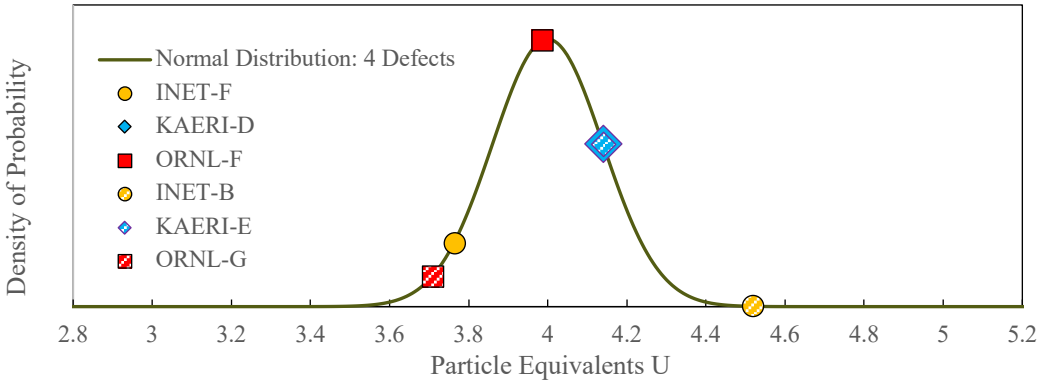

Figure 4-3. Normal distribution for uranium in simulated samples with four defects versus measured values.

In addition to representing a highly unlikely actual value for uranium content, as discussed above, the combined LBL data for uranium leached from simulated samples INET-G and INET-B were also more than half of an average kernel's inventory above the most likely mean value for two and four defective particles, respectively, and these data would typically lead to an erroneous conclusion that INET-G contained at least three defects and INET-B contained at least five defects, rather than the expected values of two and four, respectively. Because INET-G and INET-B results were high relative to the expected uranium content, their deviation was most likely associated with the accuracy of the measurement of uranium in the leachates. Conversely, the combined LBL data for uranium leached from simulated samples KAERI-F and ORNL-D were both below the 99.7% probability interval for a sample with two defective particles. For low outliers like these, either error in the uranium analysis and/or incomplete leaching could be contributing factors to the erroneous results. As discussed in the ORNL report (Hunn et

al. 2023), ORNL-D exhibited unusual postburn leaching, with 0.52 PE-U in the first postburn leach and 0.34 PE-U in the second. Because of the high amount in the second leach relative to the first leach, three more postburn leaches were conducted on ORNL-D, with 0.53 PE-U in the third leach and <0.01 PE-U in the fourth and fifth leaches. This slow leaching behavior is discussed in detail in the ORNL report, and post-LBL recovery and analysis of the two defective particles in ORNL-D revealed that the hole milled in the SiC layer to simulate a SiC defect was partially plugged in one of the particles, and residual uranium remained inside its SiC shell. Slow leaching was also observed in ORNL-G, and the postburn leach result was marginally below the 95% probability interval for four defective particles, so one or more defective particles in ORNL-G may have similarly contained residual uranium remaining after five 24 h postburn leaches. Only one postburn leach was performed on KAERI-F, so the completeness of the leaching of that sample is not known. However, given that the result of the KAERI-F postburn leach was well below the 99.7% probability interval for the sample, it is possible that plugging also occurred in that sample. There was no indication of incomplete postburn leaching of the particles with simulated defects in the INET data. It is worth noting the difference in burn temperatures used by the three participants (Table 2-1). Whether the lower burn temperature used at ORNL resulted in more prevalent plugging of the hole in the SiC layer is unknown but should be considered as a possible factor.

In most cases, >99% of the combined LBL results for leached uranium were detected in either the preburn leach stage, when exposed-kernel defects were present, or the postburn leach stage, when SiC defects were present. This differentiation allowed for the determination of not only the total number of defective particles per sample, but also the type. Table 4-3 shows the relative fractions of uranium detected in the preburn and postburn leaching of each sample. ORNL data are presented as the total fraction leached before or after the burn and in terms of the fraction detected in each 24 h leach, in parentheses. All participants achieved good discrimination for the simulated SiC defects, as 99.24–100% of the total measured uranium in each sample containing one or more SiC defects was detected in the postburn leachates. The LBL analysis at ORNL noted a small but measurable amount of uranium in the preburn leachates of ORNL-E (4.88E-6 g) and ORNL-G (7.22E-6 g) that exceeded the uranium contribution from the SRM 1632d powder added to each simulated sample by more than one order of magnitude (see Table A-6). In both ORNL-E and ORNL-G, more uranium was detected in the second preburn leach than in the first, which suggests minor premature leaching of the simulated SiC defects in those samples before the burn, as discussed in more detail in the ORNL report (Hunn et al. 2023). Similar minor premature leaching was also observed and studied during the development work for fabricating the particles with simulated SiC defects (Gerczak et al. 2022).

Table 4-3. Fraction of the Total U Measured by LBL at Various Stages of Leaching

Defect number and type	Leach stage	INET	KAERI	ORNL [a]
zero	preburn	0.03%		69.46% (63.13%, 6.33%)
defects	postburn	99.97%		30.54% (28.03%, 2.50%)
one	preburn	50.47%	99.03%	99.995% (99.64%, 0.35%)
exposed-kernel defect	postburn	49.53%	0.97%	0.005% (0.004%, 0.0004%)
two	preburn	38.92%	99.45%	99.98% (99.71%, 0.27%)
exposed-kernel defects	postburn	61.08%	0.55%	0.016% (0.016%, 0.0004%)
four	preburn	48.62%	100.00%	99.99% (99.69%, 0.30%)
exposed-kernel defects	postburn	51.38%		0.014% (0.014%, 0.0004%)
one	preburn	0.00%		0.76% (0.08%, 0.68%)
SiC defect	postburn	100.00%	100.00%	99.24% (98.93%, 0.31%)
two	preburn	0.00%		0.04% (0.04%, 0.0012%)
SiC defects	postburn	100.00%	100.00%	99.96% (37.25%, 24.11%, 37.88%, 0.36%, 0.36%)
four	preburn	0.00%		0.28% (0.018%, 0.26%)
SiC defects	postburn	100.00%	100.00%	99.72% (77.15%, 17.18%, 5.27%, 0.05%, 0.08%)

[a] ORNL data in parentheses indicate fraction in each successive leach

For the samples containing particles with simulated exposed-kernel defects, LBL analyses at KAERI and ORNL yielded the expected results: a clear demarcation between the preburn and postburn leaching of uranium was observed, which allowed the conclusion that these samples contained only exposed-kernel defects. In contrast, incomplete preburn leaching at INET resulted in only 38.9%–50.5% of the total leached uranium from the exposed-kernel defects being detected by the preburn leaching. In practice, this splitting of uranium between the preburn and postburn leaches would prevent effective discrimination between exposed-kernel and SiC defects. As discussed in the INET report (Xu and Chen 2023), this incomplete preburn leaching was likely due to the inability of the 2 h preburn leach to completely dissolve the UO_2 kernels in the particles with simulated exposed-kernel defects. Comparison of the LBL procedures listed in Table 2-1 shows that the INET preburn leaching was done for a much shorter time, at lower temperature, and at half the acid concentration compared with the parameters used at ORNL. The ORNL procedures resulted in 99.64%–99.71% of the total amount of uranium leached from the simulated exposed-kernel defects being detected in the first 24 h leach. The rate of kernel dissolution is expected to scale with the temperature and concentration of the acid. In addition, the thin cracks in the particles with simulated exposed-kernel defects (see Figure 1-1) presented a restriction in the accessibility of the acid to the kernel location, which is another factor that is expected to impact the time required for complete leaching. Given that 38.9%–50.5% of the total leached uranium from the exposed-kernel defects was removed by the 2 h preburn leach performed at INET, it is likely that a longer leaching time under the same conditions would have eventually resulted in complete leaching prior to the burn stage. In the INET analysis of the exposed-kernel defects, a second preburn leach was not performed; however, kernel dissolution was essentially completed after burning the samples and leaching for another 8 h with the same acid temperature and concentration used in the preburn. After the burn stage, the pyrocarbon layers in the particles with exposed-kernel defects were no longer present, providing more ready access of the acid to the kernel material. In addition, the UO_2 kernel would have oxidized to U_3O_8, which is more soluble in nitric acid. The KAERI preburn leaching appeared to be slightly less effective than the ORNL preburn leaching of the samples containing simulated exposed-kernel defects, based on the higher fractions (Table 4-3) and uranium masses (Table 4-1) measured in the KAERI postburn leaching. Preburn leach times were the same at KAERI and ORNL, but the acid concentration and temperature used in the analysis at KAERI were moderately lower, which may explain the difference.

For the samples with zero included particles with simulated defects, the combined LBL analysis should yield results close to the uranium impurity content in the SRM 1632d powder included in each sample, since these samples contained no other sources of uranium. The uranium in KAERI-G was reported to be below the minimum measurable value (Yeo 2024). The combined LBL result for uranium in INET-D was 3.07E-6 g, which is significantly higher than the 2.69E-7 g U contribution from the SRM 1632d standard (Table A-4). The combined LBL result for uranium in ORNL-B was 4.22E-7 g, which is closer to the 2.51E-7 g U contribution from the SRM 1632d standard (Table A-6). The larger discrepancy in the INET result may be related to the lower accuracy of the fluorescence spectrometry method compared with that of ICP-MS, especially for lower concentrations.

4.2 IMPURITY ANALYSIS BY LEACH-BURN-LEACH

The NIST SRM 1632d coal impurity standard includes many elements often specified for fuel fabrication QC acceptance testing (Al, Ca, Ti, V, Cr, Mn, Fe, Co, and Ni, and U) as well as other elements, some of which are measured during LBL of irradiated fuel (Sb, Ba, Cd, Ce, Cs, Eu, Rb, Sr, and Th). This list of elements was targeted for analysis as part of the round-robin test to provide insight into the use of LBL to monitor for and measure their presence. The concentrations of all the listed elements except for Ni were reported in the NIST SRM 1632d certificate of analysis (Mackey et al. 2011) as either certified values (i.e., those values considered to be measured with high confidence because uncertainties were determined by investigation or accounting for known or suspected sources of bias) or reference values (i.e., those values whose reported uncertainties reflected only measurement precision). The Ni concentration in the coal standard was provided as a value for information purposes only because the uncertainty was not

sufficiently accessed. Preparation of the simulated samples included the NIST-recommended procedure to homogenize and accurately determine a dry powder weight relevant to the reported reference mass fractions reported in the certificate of analysis (Gerczak et al. 2022). The reference mass fractions for the SRM 1632d powder, dry masses of powder added to each simulated sample, and mass of each listed element in the individual simulated samples are tabulated in Appendix A.

Detailed results and discussion of the LBL impurity analyses by each round-robin participant are included in their separate reports (Xu and Chen 2023; Yeo 2024; Hunn et al. 2023). Table 4-4 provides a summary of the LBL results in comparison to the known content of each listed element targeted by the round-robin experiment. For each of the seven simulated samples provided to the three round-robin participants, detection ratios were determined for each measured element by dividing the measured mass of that element by the known mass of the element in the SRM 1632d powder added to the sample, as listed in Appendix A. A detection ratio of unity would represent complete dissolution of the element and wholly accurate analysis of its presence in solution. Ratios within an analytical chemistry uncertainty of approximately ±10% of unity can be considered sufficient. Uncertainties of ±20% might be expected for lower concentrations close to the minimum detection limit (MDL). Results for individual leaches of each simulated sample are provided in the reports prepared by each participant. Table 4-4 presents the mean and standard deviation (SD) of the combined LBL results for each element across the seven simulated samples analyzed by each participant. Also included in Table 4-4 are the average mass of each listed element across all 21 simulated samples. Nonideal results are highlighted in gray and discussed below.

Table 4-4. Average Detection Ratio for Impurities Measured by LBL Versus Content in SRM 1632d Powder

Impurity Element	SRM 1632d average mass (g)	INET mean ± SD	KAERI mean ± SD	ORNL mean ± SD
Cadmium (Cd)	4.0E-08	1.09 ± 0.77	201.60 ± 121.70	1.03 ± 0.17
Europium (Eu)	1.1E-07	0.67 ± 0.19	below detection	1.12 ± 0.05
Antimony (Sb)	2.2E-07	12.00 ± 4.06	below detection	0.23 ± 0.07
Cesium (Cs)	3.0E-07	1.00 ± 0.14	below detection	1.08 ± 0.03
Thorium (Th)	7.1E-07	11.50 ± 3.45	0.12 ± 0.03	0.96 ± 0.08
Cobalt (Co)	1.7E-06	0.70 ± 0.47	0.91 ±	1.04 ± 0.04
Rubidium (Rb)	3.7E-06	1.02 ± 0.10	0.92 ±	1.04 ± 0.03
Nickel (Ni)	5.0E-06	1.27 ± 0.56	11.80 ± 8.61	1.54 ± 0.12
Cerium (Ce)	5.8E-06	0.71 ± 0.13	0.74 ± 0.09	0.96 ± 0.04
Manganese (Mn)	6.5E-06	0.74 ± 0.25	0.98 ± 0.14	1.01 ± 0.02
Chromium (Cr)	6.8E-06	0.87 ± 0.14	2.79 ± 1.99	1.10 ± 0.03
Vanadium (V)	1.2E-05	0.98 ± 0.29	0.73 ± 0.07	0.97 ± 0.02
Barium (Ba)	2.0E-05	0.82 ± 0.15	1.54 ± 0.86	1.03 ± 0.02
Strontium (Sr)	3.2E-05	0.89 ± 0.25	0.89 ± 0.09	1.03 ± 0.04
Titanium (Ti)	2.4E-04	2.25 ± 0.76	0.57 ± 0.07	0.76 ± 0.04
Calcium (Ca)	7.2E-04	not reported	not reported	0.94 ± 0.04
Iron (Fe)	3.7E-03	0.70 ± 0.30	0.92 ± 0.09	1.04 ± 0.10
Aluminum (Al)	4.5E-03	0.77 ± 0.09	0.12 ± 0.03	0.95 ± 0.04

Note: Mean values that deviated more than 10% from the expected result and abnormally high SDs that reflect large sample-to-sample variability are highlighted.

The summary results in Table 4-4 are sorted in order of impurity content. The NIST SRM 1632d coal impurity standard includes impurities of interest that varied in mass fraction over five orders of magnitude. The lower impurity concentrations provide insight into the sensitivity of the LBL analysis. The impurity concentrations of Sb, Cs, and Eu in the simulated samples were relatively low, with known masses of 1–3E-7 g, which were below the MDL of 2E-6 g for the analysis performed at KAERI. The relatively higher KAERI MDL may have been related to the use of ICP-OES, which typically has an

MDL that is three orders of magnitude higher than that of ICP-MS. The mass of Cd in the simulated samples was the lowest of the targeted impurities, ranging from 3.7E-8 g to 4.4E-8 g. The large error in the Cd result reported by KAERI may have been related to error in the analytical chemistry element identification for the signal identified as Cd, as Cd was well below the KAERI MDL. On average, analyses at INET and ORNL yielded detection ratios for Cd that were within ±10% of unity. However, the high standard deviation in the INET and ORNL summary data for Cd reflects a relatively wide variation in the results across the seven measured samples that is not unexpected given that the concentrations in the leachates were relatively low with respect to the MDL of the ICP-MS chemistry analysis. The Cd data reported by ORNL was only 6× the MDL in the first preburn leach and unmeasurable in all successive leaches (Hunn et al. 2023). The LBL analyses performed at INET and ORNL were also both successful for Cs, but Eu results were marginal, and Sb results deviated significantly from the expected content. Data discussed in the ORNL report (Hunn et al. 2023) indicate that Eu analysis may have been impacted by a relatively high background for Eu. Subtraction of this background using analyses performed on high-purity acid blanks brought the ORNL results to within a ±10% deviation from the known mass for Eu in each sample. The ORNL report also includes discussion of the Sb discrepancy, which exhibited the lowest detection ratios reported by ORNL of 0.15–0.32. Data obtained from the four successive leaches performed at ORNL on each sample indicate that Sb was relatively insoluble in hot nitric acid, as discussed further below. This finding was consistent with several reports in the literature regarding the low solubility of antimony oxides in nitric acid (Lewińska et al. 2017) and complexing with silica in the boiling vessel wall (Hewitt and Cragin 1991).

The mass of Th in the simulated samples was also below the KAERI MDL, which may explain the discrepancy in the Th detection ratio for the KAERI data. Results for Th analysis at INET were like Sb in that both yielded mass values that were more than 10× higher than the known values on average and in that the standard deviations across the seven measured samples were relatively high. The high deviation for Th and Sb between like samples suggests that the variability in the INET data was dominated by error in the analytical chemistry measurements for these relatively low concentration elements. The impurity contents of Co and Rb in the simulated samples were close to the KAERI MDL for the KAERI analyses and each was measured in only one out of seven KAERI samples. Therefore, no standard deviations for Co and Rb were available for the KAERI dataset in Table 4-4. However, the singular results obtained at KAERI were consistent with the Co and Rb content in those samples to within 10%. The ORNL results yielded detection ratios for Co and Rb that were sufficiently close to unity. The Rb detection ratios from the INET LBL were centered on unity, but the individual sample results varied from 0.87 to 1.12. The INET Co detection ratios were low on average and varied from 0.44 to 1.20, suggesting a high analytical uncertainty—as was observed for Th and Sb, but to a lesser extent.

Of the more prevalent metallic impurities targeted for analysis—all of which were sufficiently above the detection limits for the ICP-MS method—the ORNL results showed significant deviation from the expected masses for Ni and Ti only (Hunn et al. 2023). As mentioned in Appendix A, the Ni mass fraction was not a certified value. However, the relatively higher standard deviation in the Ni analysis across the seven ORNL samples suggests that the analytical chemistry results had a higher included error than that of most of the other elements. The INET detection ratios for Ni exhibited a similar relatively high variability between samples. Both the KAERI and ORNL Ti detection ratios were low but relatively consistent for all seven samples, which suggests that Ti was not completely leached during the KAERI and ORNL LBL. Conversely, the INET mean detection ratio for Ti erred on the high side and had a wide sample-to-sample spread of 1.2–3.1, which suggests that the INET results for Ti were dominated by low accuracy in the ICP-MS. For the other impurities present in the simulated sample in masses above 5E-6 g, the INET results tended to yield moderately low detection ratios with relatively high sample-to-sample variability, except for V, which had a mean detection ratio close to unity but which also varied significantly between samples. It is possible the INET results for the more prevalent impurities that showed detection ratios significantly less than unity were impacted by incomplete leaching related to the comparatively shorter leach period used at INET, coupled with the lower acid concentration (Table 2-1).

The INET and ORNL reports include discussions of the fraction of the combined LBL result for each impurity that was dissolved from each simulated sample during each leach in the LBL analyses at INET and ORNL (Xu and Chen 2023; Hunn et al. 2023). Figure 4-4 and Figure 4-5 display these fractions averaged over all seven simulated samples. The ORNL columns display results for the first and second leaches conducted during both the preburn leach stage and the postburn leach stage. Each ORNL leach was conducted for 24 h (Table 2-1). The INET columns display the fractions dissolved in a single 2 h preburn leach and a single 8 h postburn leach. The ORNL results showed that significant leaching often occurred in the second 24 h preburn leach. However, after the burn stage, which typically increases the effectiveness of leaching metallic impurities, one 24 h leach was usually sufficient. Notable exceptions were Sb, in which an average of 10% of the combined LBL total was leached in the second postburn leach, and Ti, in which an average of 1.7% of the combined LBL total was leached in the second postburn leach. These were the two elements that exhibited significantly low detection ratios in the ORNL summary analysis results (Table 4-4). The relatively high fractions leached in the second 24 h postburn leach indicate the presence of residual Sb and Ti after the burn that was inaccessible or insoluble in the hot nitric acid—especially in the case of Sb, for which the average detection ratio was only 0.23. Figure 4-4 and Figure 4-5 show that, for all elements, the two 24 h preburn leaches at ORNL leached a higher fraction of the total than the single 2 h preburn leach conducted at INET. Much of what remained after the 2 h preburn leach at INET was presumably dissolved during the 8 h postburn leach, after the burn stage removed the carbon material in the SRM 1632 powder, which should have exposed internal impurities trapped in the coal and oxidized most. However, it is unknown how much may have remained in the INET sample that could have been leached by subsequent postburn leaching. The ORNL second postburn leach data displayed in Figure 4-4 and Figure 4-5 suggest that significant amounts of at least Al, Ti, Cr, Sb, and Ba remained, as these all showed >0.5% contributions after two 24 h preburn leaches and one 24 h postburn leach had been completed. In addition, the two ORNL simulated samples subjected to five 24 h postburn leaches collected additional measurable impurities in the third, fourth, and fifth postburn leach of 0.3% Al, 1.6%–1.9% Ti, 3.0%–3.1% Cr, and 0.2%–0.3% Ba (Hunn et al. 2023).

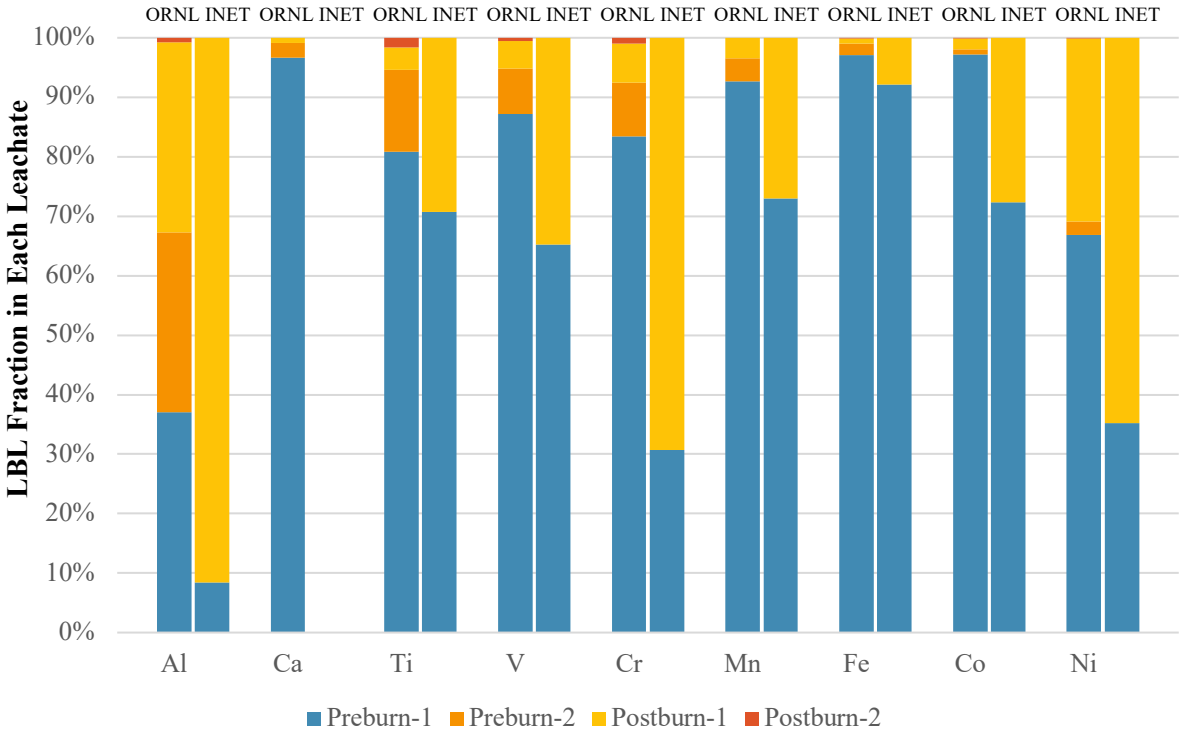

Figure 4-4. Fraction per leach for QC-relevant impurities measured in simulated samples.

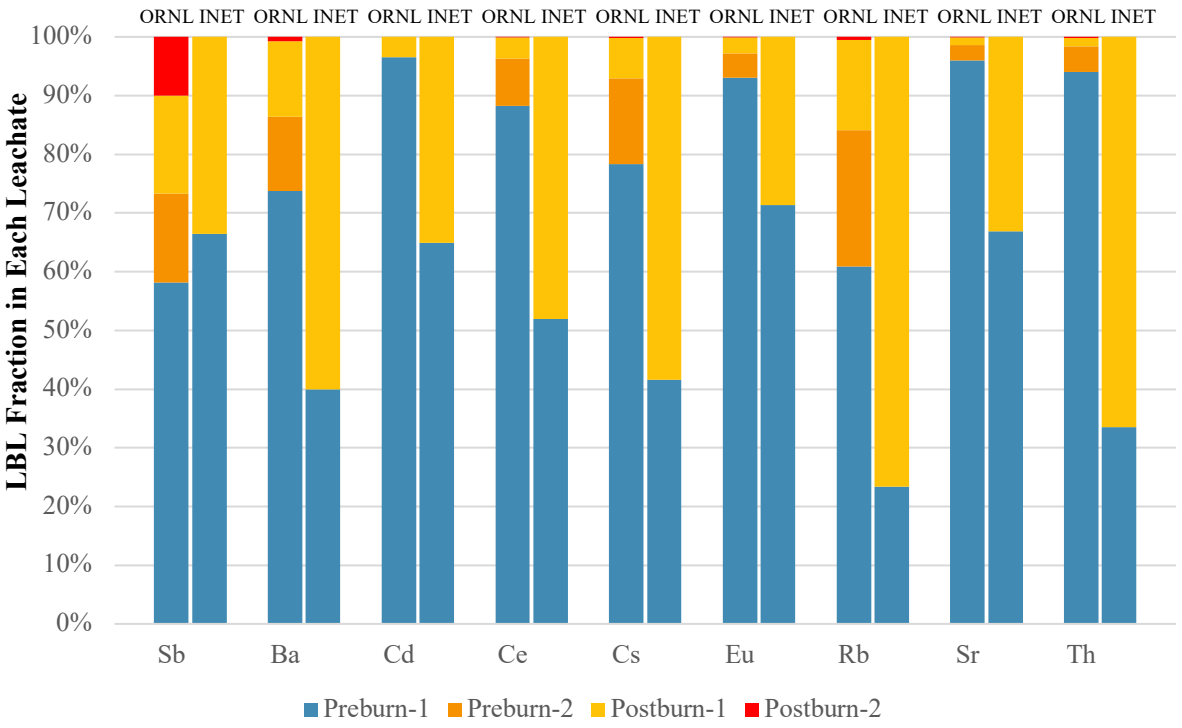

Figure 4-5. Fraction per leach for other targeted impurities measured simulated samples.

5. CONCLUSIONS

Participating organizations from three member states in the GIF Very High Temperature Reactor System Fuel and Fuel Cycle Project Management Board completed a round-robin test to benchmark and explore the consistency of the methods and results associated with LBL analyses of TRISO-coated particle fuel. The round-robin test included representative sublots, provided by INET, of TRISO particles with depleted UO_2 kernels that were fabricated in a production-scale coater. The representative sublots were analyzed by ORNL and INET, and their LBL results for uranium were compared and are reported herein. A second round-robin sample set was prepared for each participant by ORNL that contained known quantities of particles with simulated defects, as well as measured amounts of a NIST-certified coal impurity standard (Gerczak et al. 2022). These simulated samples provided for quantitative analysis of the accuracy of the different LBL methods applied by each organization. Each simulated sample contained one, two, or four uranium-bearing TRISO particles with simulated defects hidden among ~10,000 nonuranium-bearing coated particles. The purpose of the simulated samples was to use the simulated exposed-kernel defects and simulated SiC defects to test the accuracy of the LBL methods used by each participant for detecting and enumerating these types of defects. In addition, the included coal standard provides independently certified concentrations of many elements of interest to TRISO fuel performance and served as a benchmark for evaluation of the capability of the different LBL methods used by each participant for measuring various metallic impurities. After completion of LBL by all participating institutions, a copy of the information in Appendix A revealing the number of simulated defects and the masses of the various impurities contained in each round-robin sample was provided to each round-robin participant. Each participant issued a report describing the LBL processes they used for the round-robin test and the details of their measurement results (Xu and Chen 2023; Yeo 2024; Hunn et al. 2023). Reported herein are summary comparisons of the results of each participant's LBL analyses of the simulated samples and discussion of factors that may have contributed to observed differences and discrepancies with the known values in the simulated samples.

Section 2 includes an overview table of the key parameters used in each participant's LBL procedure (Table 2-1). All participants used hot nitric acid to leach the samples before and after a burn stage. Acid concentration, temperature, and leaching time varied among participants. Both acid concentration and temperature are expected to impact the rate that uranium and various impurity elements are dissolved in the leaching acid, and the combination of leaching rate and time determines the effectiveness of each leaching step. As discussed below, some differences in LBL results from this round-robin test were related to differences in the leaching parameters. All participants heated the particles in air, but time and temperature varied. Burn temperatures ranged from 750°C to 850°C, all of which are above the oxidation temperature of carbon in air. Burn times ranged from 10 h to 72 h. The combination of temperature and time will impact the rate of oxidation. There were no strong indicators that the differences in the burn parameters impacted the LBL results in this round-robin test. Analytical chemistry methods also varied between participants, and the different accuracy of these methods appeared to influence the accuracy of the LBL results, especially in cases where the concentrations of some elements of interest in the leachates were low.

Section 3 includes a comparison of LBL analyses completed at INET and ORNL for exposed uranium in the representative sublots. No TRISO particles with exposed-kernel defects or SiC defects were detected in any of the three representative sublots inspected with LBL at each facility. The highest detected particle equivalent value of uranium was less than 0.01 for a sample of ~31,000 particles measured by ORNL, and this is well below what would be associated with an exposed-kernel defect or a SiC defect. However, measurable uranium concentrations in the leachates from the representative sublots were present and reported by both participants (Table 3-1). The mass fraction of uranium measured by LBL in the representative sublots examined at ORNL exhibited an order of magnitude range of 0.013–0.150 ppm. The LBL analyses at INET yielded total mass fractions of 0.050–0.085 ppm U. Some of the observed variation in measured uranium mass fraction may have been associated with the uncertainty in measuring

these relatively low concentrations of uranium. However, given that the 0.150 ppm result for one of the representative sublots measured at ORNL was well above the MDL and clearly higher than the LBL results for the other five sublots, that sample may have included discrete uranium contamination that was perhaps localized to a single particle, such as that which would come from a tiny kernel fragment included in the OPyC layer, as opposed to dispersed uranium contamination evenly distributed throughout the parent batch.

Section 4.1 provides a summary of the round-robin LBL results for uranium (Table 4-1). Several issues were noted. Ideally, uranium in particles with exposed-kernel defects should be detected in the preburn leach stage and uranium in particles with SiC defects should be detected in the postburn leach stage. Table 4-3 shows the fraction of uranium detected before and after the burn stage. The preburn leach procedures at KAERI and ORNL were effective in leaching 99% or more of the total measured uranium from particles with exposed-kernel defects using a leaching time of 48 h and 60–70% concentrated nitric acid. The preburn leach procedure used at INET differed from the others by using lower concentration acid (35%) and a preburn leaching time of only 2 h, which was unable to dissolve all the acid from the particles with exposed-kernel defects. Roughly half of the total measured uranium from particles with exposed-kernel defects in the simulated samples analyzed at INET was not leached until after the burn. This was a valuable round-robin test observation, as it demonstrated the importance of using a sufficient combination of acid concentration, temperature, and time in the preburn leach stage if discrimination between exposed-kernel defects and SiC defects is desired.

Another issue evident in the summary results in Table 4-1 was unexpected deviation from whole number values for the measured particle equivalents of uranium. Some deviation is expected due to uncertainties in the analytical chemistry analysis of the uranium concentration in each leachate (estimated to be roughly ±10%). Additional deviation is expected due to variability in the actual uranium content in each particle with a simulated defect. The PE-U values were determined by dividing by the measured average uranium mass per particle. The impact of uranium in the selected particles being above or below this average was considered statistically in the discussion in Section 4.1. Most of the observed deviation from whole number values for the measured particle equivalents of uranium in each simulated sample could be accounted for by the combination of the analytical chemistry uncertainty and statistically probable variation in uranium content. However, at least two cases of erroneously high and two cases of erroneously low uranium content were not sufficiently accounted for by these two expected causes. Samples ORNL-D and KAERI-F each contained two particles with simulated SiC defects, but postburn leaching only detected 1.40 PE-U and 1.57 PE-U, respectively. Table 4-3 shows that ORNL-D exhibited unusually delayed leaching after the burn, with significant fractions detected in three successive 24 h postburn leaches. The particles in ORNL-D were analyzed with XCT after leaching, and it was discovered that the FIB-milled hole in the SiC had become occluded during the postburn leaching. ORNL-G, which contained four particles with a simulated SiC defect, showed similar slow leaching spanning three successive 24 h postburn leaches, suggesting that its leaching was also hampered by occlusion of the hole in the SiC. Details of the mechanism for plugging of the FIB-milled hole are unknown, but the issue may be more related to the efficacy of the chosen method for simulation of a SiC defect than deficiencies in the LBL process.

Results for INET-G and INET-B were erroneously high, which is an error that cannot be explained by insufficiencies in the leaching parameters or simulated sample preparation. It is likely that the higher-than-expected deviations in these two samples were related to an elevated uncertainty in the analysis of uranium by laser fluorescence spectrometry versus ICP-MS. Figure 4-3 shows that INET-B, which contained four particles with a simulated SiC defect, only marginally exceeded the range of more probable uranium content. This small margin could be accounted for by an elevated uncertainty of 10%–20% in the analysis of uranium concentration in the postburn leachate. In contrast, INET-G was more than 30% beyond the probable range for uranium content in one particle with a simulated SiC defect (Figure 4-1).

Section 4.2 provides a summary of the LBL analysis results for the list of targeted impurities contained in the NIST SRM 1632d coal impurity standard added to each simulated sample (see Appendix A). The targeted impurities varied in mass fraction by over five orders of magnitude, which provided an opportunity to consider the sensitivity of the LBL analysis methods. Results are summarized in Table 4-4 in terms of the average detection ratio across the seven simulated samples measured by each participant, in which a detection ratio of unity would be achieved by complete dissolution of the element and wholly accurate analysis of its presence in solution. As discussed in Section 4.2, the MDL of 2E-6 g for the analyses performed at KAERI was higher than that obtained via ICP-MS by the other two participants. This relatively higher MDL impacted measurement of elements present in quantities of ≤5E-6 g. Elements present in the lower concentrations also challenged the analyses at INET and ORNL, although impact varied. Both INET and ORNL were able to obtain an average detection ratio within 10% of unity for Cd, which was the least prevalent targeted element at 4E-8 g on average. However, sample-to-sample variation in the measured Cd was relatively high. In general, the elements present in higher concentrations resulted in smaller standard deviations in the detection ratios across the seven-sample set. The overall INET detection ratios for the targeted elements present in quantities well above the MDL tended to be more than 10% below unity, which suggested that the dissolution of these elements may have been incomplete because of the relatively shorter time, lower temperature, and lower acid concentration compared with the parameters used at ORNL, which typically yielded values closer to unity.

Figure 4-4 and Figure 4-5 provide insight into the solubility of the various analyzed elements during hot acid leaching at INET and ORNL. These figures show the fraction of the total leached quantity that was measured in each successive leach. Comparison between the INET and ORNL results in these figures highlights the impact of the difference in leaching concentration, temperature, and time used by these two participants on the fraction leached prior to the burn. The multiple preburn and postburn leaches performed at ORNL also highlight the variable solubility for the different elements. For instance, Al exhibited the lowest preburn solubility but was effectively dissolved in the samples analyzed at ORNL after the burn. Leaching of Sb was unique in that it evidently had very low solubility. Low solubility of Sb in nitric acid has been reported in the literature, and aqua regia has been recommended as an effective alternative to nitric acid for Sb digestion (Lewińska et al. 2017). After Sb, Ti exhibited the next lowest solubility and the next highest leach fraction in the second 24 h postburn leach performed at ORNL.

6. REFERENCES

Gerczak, Tyler J., Charles A. Baldwin, Grant Helmreich, John D. Hunn, and Fred C. Montgomery. 2022. *Preparation of Simulated LBL Defects for Round-Robin Experiment*. ORNL/TM-2015/722, Revision 3. Oak Ridge: Oak Ridge National Laboratory.

Hewitt, Alan D., and James H. Cragin. 1991. "Comment on 'Acid Digestion for Sediments, Sludges, Soils, and Solid Wastes. A Proposed Alternative to EPA SW 846 Method 3050.'" Environmental Science Technology 25(5): 985–986.

Hunn, John D. 2004. *Data Summary for Nominal 500 µm DUO_2 kernels*. ORNL/CF-04/04, Revision 0. Oak Ridge: Oak Ridge National Laboratory.

Hunn, John D., Tyler J. Gerczak, Fred C. Montgomery, and Grant W. Helmreich. 2023. *ORNL Analysis of Leach-Burn-Leach Round-Robin Test Samples*. ORNL/TM-2024/2951, Revision 0. Oak Ridge: Oak Ridge National Laboratory.

Lewińska, Karolina, Anna Karczewska, Marcin Siepak, Bernard Gałka, Michal Stysz, and Cezary Kaźmierowski. 2017. "Recovery and Leachability of Antimony from Mine and Shooting Range Soils." *Journal of Elementology* 22(1): 79–90.

Mackey, Elizabeth A., et al. 2011. *Certificate of Analysis Standard Reference Material 1632d Trace Elements in Coal*. Certificate issue date: October 14, 2014. Gaithersburg: National Institute of Standards and Technology.

Yeo, Sunghwan. 2024. *Leach Burn Leach Results of Round Robin Experiment*. Daejoen: Korea Atomic Energy Research Institute. An Excel workbook containing supplemental information used herein to construct summary tables was also provided to the author by email.

Xu, Gang, and Xiaotong Chen. 2023. *INET Analysis of Leach-Burn-Leach Round-Robin Test Samples*. Beijing: Institute of Nuclear and New Energy Technology. An Excel workbook containing supplemental information used herein to construct summary tables was also provided to the author by email.

APPENDIX A. SEEDED DEFECTS AND IMPURITIES IN SIMULATED SAMPLES

After completion of LBL analysis by all participating institutions, additional information was added to the report, *Preparation of Simulated LBL Defects for Round-Robin Experiment* (Gerczak et al. 2022), to document the number and type of particles with simulated defects that were added to each sample set, as well as the mass of each trace element from the added standard reference material—SRM 1632d. Table A-1 through Table A-3 identify the specific particles with simulated defects contained in the simulated samples analyzed at INET, KAERI, and ORNL, respectively. Detailed information on these particles and images of the defect microstructure of each can be found in the original report (Gerczak et al. 2022).

Table A-1. Identification of Number and Type of Simulated Defects Added to Each INET Sample

Test sample	Number of simulated defects added	Type of simulated defect added	Particles added
INET-A	2	simulated exposed-kernel defect	GIF-03, GIF-06
INET-B	4	simulated SiC defect	FIB-06, FIB-07, FIB-08, FIB-09
INET-C	2	simulated SiC defect	FIB-03, FIB-05
INET-D	0	none	none
INET-E	1	simulated exposed-kernel defect	GIF-02
INET-F	4	simulated exposed-kernel defect	GIF-07, GIF-09, GIF-14, GIF-15
INET-G	1	simulated SiC defect	FIB-02

Table A-2. Identification of Number and Type of Simulated Defects Added to Each KAERI Sample

Test sample	Number of simulated defects added	Type of simulated defect added	Particles added
KAERI-A	2	simulated exposed-kernel defect	GIF-19, GIF-27
KAERI-B	1	simulated exposed-kernel defect	GIF-17
KAERI-C	1	simulated SiC defect	FIB-10
KAERI-D	4	simulated exposed-kernel defect	GIF-28, GIF-29. GIF-38, GIF-39
KAERI-E	4	simulated SiC defect	FIB-14, FIB-15, FIB-16, FIB-17
KAERI-F	2	simulated SiC defect	FIB-11, FIB-13
KAERI-G	0	none	none

Table A-3. Identification of Number and Type of Simulated Defects Added to Each ORNL Sample

Test sample	Number of simulated defects added	Type of simulated defect added	Particles added
ORNL-A	2	simulated exposed-kernel defect	GIF-41, GIF-42
ORNL-B	0	none	none
ORNL-C	1	simulated exposed-kernel defect	GIF-30
ORNL-D	2	simulated SiC defect	FIB-20, FIB-21
ORNL-E	1	simulated SiC defect	FIB-19
ORNL-F	4	simulated exposed-kernel defect	GIF-43, GIF-44, GIF-49, GIF-04
ORNL-G	4	simulated SiC defect	FIB-23, FIB-25, FIB-26, FIB-27

Table A-4 through Table A-6 list the amount of dried SRM 1632d reference material that was added to each simulated sample and the corresponding mass of each measured impurity calculated by multiplying the NIST-reported impurity mass fraction by the measured mass of added SRM 1632d powder. The uncertainty in each calculated impurity mass was propagated from the uncertainties in the mass fraction and measured powder mass. The NIST-reported impurity mass fractions and uncertainties come from the SRM 1632d certificate of analysis (Mackey et al. 2011), which is maintained by NIST and available online at https://www-s.nist.gov/srmors/certificates/archives/1632d.pdf. The certificate of analysis provides detailed information on the standard reference material, including the mass fractions and uncertainties for each element listed in Table A-4 through Table A-6. Certified values are values reported to have the highest confidence for accuracy because all known or suspected biases have been considered. Reference values have uncertainties that may be based only on measurement precision, and some sources of uncertainty may not be included. Information values were provided by NIST as they may be of interest and use, but these values were not reported with uncertainties due to insufficient information; therefore, uncertainties for these values are listed in the table as not applicable (NA). Preparation of the LBL round-robin simulated samples included acid washing of the ZrO_2-TRISO particles used as a sample base to which the particles with simulated defects and SRM 1632d powder were added. Thus, the impurities listed in the table should dominate the mass of impurities in each simulated sample, with the exception of uranium for the samples that include simulated defects. The uranium leached from those samples should be dominated by the uranium in the kernels of the particles with simulated defects. The average uranium content in the DUO_2 particles used to make the simulated defects (7.003E-4 g) was ~2600× that of the uranium from the SRM 1632d powder included in each sample.

Table A-4. Impurity Content in SRM 1632d Added to Each INET Simulated Sample

NIST SRM1632d Data			INET-A	INET-B	INET-C	INET-D	INET-E	INET-F	INET-G
Mass of dried SRM1632d powder added (g):			0.4945 ± 0.0005	0.5009 ± 0.0005	0.4849 ± 0.0005	0.5206 ± 0.0005	0.5076 ± 0.0005	0.4960 ± 0.0005	0.4911 ± 0.0005
Element	Quality	SRM1632 mass fraction	Mass in sample (g)	Mass in sample (g)	Mass in sample (g)	Mass in sample (g)	Mass in sample (g)	Mass in sample (g)	Mass in sample (g)
Al	reference	9.12E-03 ± 5E-05	4.51E-03 ± 2.5E-05	4.57E-03 ± 2.5E-05	4.42E-03 ± 2.5E-05	4.75E-03 ± 2.6E-05	4.63E-03 ± 2.6E-05	4.52E-03 ± 2.5E-05	4.48E-03 ± 2.5E-05
As	reference	6.1E-06 ± 2E-07	3.02E-06 ± 9.9E-08	3.06E-06 ± 1.0E-07	2.96E-06 ± 9.7E-08	3.18E-06 ± 1.0E-07	3.10E-06 ± 1.0E-07	3.03E-06 ± 9.9E-08	3.00E-06 ± 9.8E-08
B	reference	6.2E-05 ± 1E-06	3.07E-05 ± 5.0E-07	3.11E-05 ± 5.0E-07	3.01E-05 ± 4.9E-07	3.23E-05 ± 5.2E-07	3.15E-05 ± 5.1E-07	3.08E-05 ± 5.0E-07	3.04E-05 ± 4.9E-07
Ba	certified	4.042E-05 ± 8.9E-07	2.00E-05 ± 4.4E-07	2.02E-05 ± 4.5E-07	1.96E-05 ± 4.3E-07	2.10E-05 ± 4.6E-07	2.05E-05 ± 4.5E-07	2.00E-05 ± 4.4E-07	1.98E-05 ± 4.4E-07
C	reference	7.688E-01 ± 1.5E-03	3.80E-01 ± 8.3E-04	3.85E-01 ± 8.4E-04	3.73E-01 ± 8.2E-04	4.00E-01 ± 8.7E-04	3.90E-01 ± 8.5E-04	3.81E-01 ± 8.4E-04	3.78E-01 ± 8.3E-04
Ca	reference	1.44E-03 ± 3E-05	7.12E-04 ± 1.5E-05	7.21E-04 ± 1.5E-05	6.98E-04 ± 1.5E-05	7.50E-04 ± 1.6E-05	7.31E-04 ± 1.5E-05	7.14E-04 ± 1.5E-05	7.07E-04 ± 1.5E-05
Cd	reference	8E-08 ± 1E-08	3.96E-08 ± 4.9E-09	4.01E-08 ± 5.0E-09	3.88E-08 ± 4.8E-09	4.17E-08 ± 5.2E-09	4.06E-08 ± 5.1E-09	3.97E-08 ± 5.0E-09	3.93E-08 ± 4.9E-09
Ce	reference	1.17E-05 ± 4E-07	5.79E-06 ± 2.0E-07	5.86E-06 ± 2.0E-07	5.67E-06 ± 1.9E-07	6.09E-06 ± 2.1E-07	5.94E-06 ± 2.0E-07	5.80E-06 ± 2.0E-07	5.75E-06 ± 2.0E-07
Cl	certified	1.142E-03 ± 1.1E-05	5.65E-04 ± 5.5E-06	5.72E-04 ± 5.5E-06	5.54E-04 ± 5.4E-06	5.95E-04 ± 5.8E-06	5.80E-04 ± 5.6E-06	5.66E-04 ± 5.5E-06	5.61E-04 ± 5.4E-06
Co	certified	3.424E-06 ± 4.8E-08	1.69E-06 ± 2.4E-08	1.71E-06 ± 2.4E-08	1.66E-06 ± 2.3E-08	1.78E-06 ± 2.5E-08	1.74E-06 ± 2.4E-08	1.70E-06 ± 2.4E-08	1.68E-06 ± 2.4E-08
Cr	reference	1.37E-05 ± 1E-07	6.77E-06 ± 5.0E-08	6.86E-06 ± 5.1E-08	6.64E-06 ± 4.9E-08	7.13E-06 ± 5.3E-08	6.95E-06 ± 5.1E-08	6.79E-06 ± 5.0E-08	6.73E-06 ± 5.0E-08
Cs	reference	5.98E-07 ± 6E-09	2.96E-07 ± 3.0E-09	3.00E-07 ± 3.0E-09	2.90E-07 ± 2.9E-09	3.11E-07 ± 3.1E-09	3.04E-07 ± 3.1E-09	2.97E-07 ± 3.0E-09	2.94E-07 ± 3.0E-09
Cu	certified	5.83E-06 ± 3.1E-07	2.88E-06 ± 1.5E-07	2.92E-06 ± 1.6E-07	2.83E-06 ± 1.5E-07	3.04E-06 ± 1.6E-07	2.96E-06 ± 1.6E-07	2.89E-06 ± 1.5E-07	2.86E-06 ± 1.5E-07
Dy	information	9E-07 ± NA	4.45E-07 ± NA	4.51E-07 ± NA	4.36E-07 ± NA	4.69E-07 ± NA	4.57E-07 ± NA	4.46E-07 ± NA	4.42E-07 ± NA
Eu	reference	2.17E-07 ± 6E-09	1.07E-07 ± 3.0E-09	1.09E-07 ± 3.0E-09	1.05E-07 ± 2.9E-09	1.13E-07 ± 3.1E-09	1.10E-07 ± 3.0E-09	1.08E-07 ± 3.0E-09	1.07E-07 ± 2.9E-09
Fe	certified	7.49E-03 ± 1.6E-04	3.70E-03 ± 7.9E-05	3.75E-03 ± 8.0E-05	3.63E-03 ± 7.8E-05	3.90E-03 ± 8.3E-05	3.80E-03 ± 8.1E-05	3.71E-03 ± 7.9E-05	3.68E-03 ± 7.9E-05
H	certified	5.10E-02 ± 5E-04	2.52E-02 ± 2.5E-04	2.55E-02 ± 2.5E-04	2.47E-02 ± 2.4E-04	2.66E-02 ± 2.6E-04	2.59E-02 ± 2.6E-04	2.53E-02 ± 2.5E-04	2.50E-02 ± 2.5E-04
Hf	information	5E-07 ± NA	2.47E-07 ± NA	2.50E-07 ± NA	2.42E-07 ± NA	2.60E-07 ± NA	2.54E-07 ± NA	2.48E-07 ± NA	2.46E-07 ± NA
Hg	certified	9.28E-08 ± 3.3E-09	4.59E-08 ± 1.6E-09	4.65E-08 ± 1.7E-09	4.50E-08 ± 1.6E-09	4.83E-08 ± 1.7E-09	4.71E-08 ± 1.7E-09	4.60E-08 ± 1.6E-09	4.56E-08 ± 1.6E-09
K	certified	1.094E-03 ± 2.6E-05	5.41E-04 ± 1.3E-05	5.48E-04 ± 1.3E-05	5.30E-04 ± 1.3E-05	5.70E-04 ± 1.4E-05	5.55E-04 ± 1.3E-05	5.43E-04 ± 1.3E-05	5.37E-04 ± 1.3E-05
La	information	6E-06 ± NA	2.97E-06 ± NA	3.01E-06 ± NA	2.91E-06 ± NA	3.12E-06 ± NA	3.05E-06 ± NA	2.98E-06 ± NA	2.95E-06 ± NA
Mg	reference	3.90E-04 ± 6E-06	1.93E-04 ± 3.0E-06	1.95E-04 ± 3.0E-06	1.89E-04 ± 2.9E-06	2.03E-04 ± 3.1E-06	1.98E-04 ± 3.1E-06	1.93E-04 ± 3.0E-06	1.92E-04 ± 3.0E-06
Mn	reference	1.31E-05 ± 4E-07	6.48E-06 ± 2.0E-07	6.56E-06 ± 2.0E-07	6.35E-06 ± 1.9E-07	6.82E-06 ± 2.1E-07	6.65E-06 ± 2.0E-07	6.50E-06 ± 2.0E-07	6.43E-06 ± 2.0E-07
N	reference	1.59E-02 ± 1E-04	7.86E-03 ± 5.0E-05	7.96E-03 ± 5.1E-05	7.71E-03 ± 4.9E-05	8.28E-03 ± 5.3E-05	8.07E-03 ± 5.1E-05	7.89E-03 ± 5.0E-05	7.81E-03 ± 5.0E-05
Na	certified	2.969E-04 ± 4.2E-06	1.47E-04 ± 2.1E-06	1.49E-04 ± 2.1E-06	1.44E-04 ± 2.0E-06	1.55E-04 ± 2.2E-06	1.51E-04 ± 2.1E-06	1.47E-04 ± 2.1E-06	1.46E-04 ± 2.1E-06
Ni	information	1.0E-05 ± NA	4.95E-06 ± NA	5.01E-06 ± NA	4.85E-06 ± NA	5.21E-06 ± NA	5.08E-06 ± NA	4.96E-06 ± NA	4.91E-06 ± NA
Pb	certified	3.845E-06 ± 4.2E-08	1.90E-06 ± 2.1E-08	1.93E-06 ± 2.1E-08	1.86E-06 ± 2.0E-08	2.00E-06 ± 2.2E-08	1.95E-06 ± 2.1E-08	1.91E-06 ± 2.1E-08	1.89E-06 ± 2.1E-08
Rb	certified	7.36E-06 ± 2.0E-07	3.64E-06 ± 9.9E-08	3.69E-06 ± 1.0E-07	3.57E-06 ± 9.7E-08	3.83E-06 ± 1.0E-07	3.74E-06 ± 1.0E-07	3.65E-06 ± 9.9E-08	3.61E-06 ± 9.8E-08
S	certified	1.462E-02 ± 7.4E-04	7.23E-03 ± 3.7E-04	7.32E-03 ± 3.7E-04	7.09E-03 ± 3.6E-04	7.61E-03 ± 3.9E-04	7.42E-03 ± 3.8E-04	7.25E-03 ± 3.7E-04	7.18E-03 ± 3.6E-04
Sb	certified	4.45E-07 ± 1.5E-08	2.20E-07 ± 7.4E-09	2.23E-07 ± 7.5E-09	2.16E-07 ± 7.3E-09	2.32E-07 ± 7.8E-09	2.26E-07 ± 7.6E-09	2.21E-07 ± 7.4E-09	2.19E-07 ± 7.4E-09
Sc	reference	2.89E-06 ± 3E-08	1.43E-06 ± 1.5E-08	1.45E-06 ± 1.5E-08	1.40E-06 ± 1.5E-08	1.50E-06 ± 1.6E-08	1.47E-06 ± 1.5E-08	1.43E-06 ± 1.5E-08	1.42E-06 ± 1.5E-08
Se	reference	1.29E-06 ± 3E-08	6.38E-07 ± 1.5E-08	6.46E-07 ± 1.5E-08	6.26E-07 ± 1.5E-08	6.72E-07 ± 1.6E-08	6.55E-07 ± 1.5E-08	6.40E-07 ± 1.5E-08	6.33E-07 ± 1.5E-08
Si	reference	1.65E-02 ± 3E-04	8.16E-03 ± 1.5E-04	8.26E-03 ± 1.5E-04	8.00E-03 ± 1.5E-04	8.59E-03 ± 1.6E-04	8.38E-03 ± 1.5E-04	8.18E-03 ± 1.5E-04	8.10E-03 ± 1.5E-04
Sm	information	1E-06 ± NA	4.95E-07 ± NA	5.01E-07 ± NA	4.85E-07 ± NA	5.21E-07 ± NA	5.08E-07 ± NA	4.96E-07 ± NA	4.91E-07 ± NA
Sr	certified	6.35E-05 ± 1.2E-06	3.14E-05 ± 5.9E-07	3.18E-05 ± 6.0E-07	3.08E-05 ± 5.8E-07	3.31E-05 ± 6.3E-07	3.22E-05 ± 6.1E-07	3.15E-05 ± 6.0E-07	3.12E-05 ± 5.9E-07
Th	certified	1.428E-06 ± 3.5E-08	7.06E-07 ± 1.7E-08	7.15E-07 ± 1.8E-08	6.92E-07 ± 1.7E-08	7.43E-07 ± 1.8E-08	7.25E-07 ± 1.8E-08	7.08E-07 ± 1.7E-08	7.01E-07 ± 1.7E-08
Ti	certified	4.77E-04 ± 1.0E-05	2.36E-04 ± 5.0E-06	2.39E-04 ± 5.0E-06	2.31E-04 ± 4.9E-06	2.48E-04 ± 5.2E-06	2.42E-04 ± 5.1E-06	2.37E-04 ± 5.0E-06	2.34E-04 ± 4.9E-06
U	certified	5.17E-07 ± 1.2E-08	2.56E-07 ± 5.9E-09	2.59E-07 ± 6.0E-09	2.51E-07 ± 5.8E-09	2.69E-07 ± 6.3E-09	2.62E-07 ± 6.1E-09	2.56E-07 ± 6.0E-09	2.54E-07 ± 5.9E-09
V	certified	2.374E-05 ± 1.0E-07	1.17E-05 ± 5.1E-08	1.19E-05 ± 5.1E-08	1.15E-05 ± 5.0E-08	1.24E-05 ± 5.3E-08	1.21E-05 ± 5.2E-08	1.18E-05 ± 5.1E-08	1.17E-05 ± 5.0E-08
Zn	reference	1.29E-05 ± 1.2E-06	6.38E-06 ± 5.9E-07	6.46E-06 ± 6.0E-07	6.26E-06 ± 5.8E-07	6.72E-06 ± 6.2E-07	6.55E-06 ± 6.1E-07	6.40E-06 ± 6.0E-07	6.33E-06 ± 5.9E-07

Note: Listed values for mass fraction ± uncertainty were obtained from NIST SRM 1632d Certificate of Analysis (https://www-s.nist.gov/srmors/certificates/archives/1632d.pdf).
Note: Listed values for mass in sample ± uncertainty were calculated from mass fraction data and measured mass of dry powder added to each simulated sample.
Note: Elements studied in the round-robin test are highlighted yellow for QC-relevant impurities and blue for other tracked elements, including those of interest for PIE.

Table A-5. Impurity Content in SRM 1632d Added to Each KAERI Simulated Sample

NIST SRM1632d Data			KAERI-A	KAERI-B	KAERI-C	KAERI-D	KAERI-E	KAERI-F	KAERI-G
Mass of dried SRM1632d powder added (g):			0.4887 ± 0.0005	0.4860 ± 0.0005	0.5045 ± 0.0005	0.4895 ± 0.0005	0.5006 ± 0.0005	0.4922 ± 0.0005	0.4905 ± 0.0005
Element	Quality	SRM1632 mass fraction	Mass in sample (g)	Mass in sample (g)	Mass in sample (g)	Mass in sample (g)	Mass in sample (g)	Mass in sample (g)	Mass in sample (g)
Al	reference	9.12E-03 ± 5E-05	4.46E-03 ± 2.5E-05	4.43E-03 ± 2.5E-05	4.60E-03 ± 2.6E-05	4.46E-03 ± 2.5E-05	4.57E-03 ± 2.5E-05	4.49E-03 ± 2.5E-05	4.47E-03 ± 2.5E-05
As	reference	6.1E-06 ± 2E-07	2.98E-06 ± 9.8E-08	2.96E-06 ± 9.7E-08	3.08E-06 ± 1.0E-07	2.99E-06 ± 9.8E-08	3.05E-06 ± 1.0E-07	3.00E-06 ± 9.8E-08	2.99E-06 ± 9.8E-08
B	reference	6.2E-05 ± 1E-06	3.03E-05 ± 4.9E-07	3.01E-05 ± 4.9E-07	3.13E-05 ± 5.1E-07	3.03E-05 ± 4.9E-07	3.10E-05 ± 5.0E-07	3.05E-05 ± 4.9E-07	3.04E-05 ± 4.9E-07
Ba	certified	4.042E-05 ± 8.9E-07	1.98E-05 ± 4.4E-07	1.96E-05 ± 4.3E-07	2.04E-05 ± 4.5E-07	1.98E-05 ± 4.4E-07	2.02E-05 ± 4.5E-07	1.99E-05 ± 4.4E-07	1.98E-05 ± 4.4E-07
C	reference	7.688E-01 ± 1.5E-03	3.76E-01 ± 8.2E-04	3.74E-01 ± 8.2E-04	3.88E-01 ± 8.5E-04	3.76E-01 ± 8.3E-04	3.85E-01 ± 8.4E-04	3.78E-01 ± 8.3E-04	3.77E-01 ± 8.3E-04
Ca	reference	1.44E-03 ± 3E-05	7.04E-04 ± 1.5E-05	7.00E-04 ± 1.5E-05	7.26E-04 ± 1.5E-05	7.05E-04 ± 1.5E-05	7.21E-04 ± 1.5E-05	7.09E-04 ± 1.5E-05	7.06E-04 ± 1.5E-05
Cd	reference	8E-08 ± 1E-08	3.91E-08 ± 4.9E-09	3.89E-08 ± 4.9E-09	4.04E-08 ± 5.0E-09	3.92E-08 ± 4.9E-09	4.00E-08 ± 5.0E-09	3.94E-08 ± 4.9E-09	3.92E-08 ± 4.9E-09
Ce	reference	1.17E-05 ± 4E-07	5.72E-06 ± 2.0E-07	5.69E-06 ± 1.9E-07	5.90E-06 ± 2.0E-07	5.73E-06 ± 2.0E-07	5.86E-06 ± 2.0E-07	5.76E-06 ± 2.0E-07	5.74E-06 ± 2.0E-07
Cl	certified	1.142E-03 ± 1.1E-05	5.58E-04 ± 5.4E-06	5.55E-04 ± 5.4E-06	5.76E-04 ± 5.6E-06	5.59E-04 ± 5.4E-06	5.72E-04 ± 5.5E-06	5.62E-04 ± 5.4E-06	5.60E-04 ± 5.4E-06
Co	certified	3.424E-06 ± 4.8E-08	1.67E-06 ± 2.4E-08	1.66E-06 ± 2.3E-08	1.73E-06 ± 2.4E-08	1.68E-06 ± 2.4E-08	1.71E-06 ± 2.4E-08	1.69E-06 ± 2.4E-08	1.68E-06 ± 2.4E-08
Cr	reference	1.37E-05 ± 1E-07	6.70E-06 ± 4.9E-08	6.66E-06 ± 4.9E-08	6.91E-06 ± 5.1E-08	6.71E-06 ± 4.9E-08	6.86E-06 ± 5.1E-08	6.74E-06 ± 5.0E-08	6.72E-06 ± 5.0E-08
Cs	reference	5.98E-07 ± 6E-09	2.92E-07 ± 2.9E-09	2.91E-07 ± 2.9E-09	3.02E-07 ± 3.0E-09	2.93E-07 ± 3.0E-09	2.99E-07 ± 3.0E-09	2.94E-07 ± 3.0E-09	2.93E-07 ± 3.0E-09
Cu	certified	5.83E-06 ± 3.1E-07	2.85E-06 ± 1.5E-07	2.83E-06 ± 1.5E-07	2.94E-06 ± 1.6E-07	2.85E-06 ± 1.5E-07	2.92E-06 ± 1.6E-07	2.87E-06 ± 1.5E-07	2.86E-06 ± 1.5E-07
Dy	information	9E-07 ± NA	4.40E-07 ± NA	4.37E-07 ± NA	4.54E-07 ± NA	4.41E-07 ± NA	4.51E-07 ± NA	4.43E-07 ± NA	4.41E-07 ± NA
Eu	reference	2.17E-07 ± 6E-09	1.06E-07 ± 2.9E-09	1.05E-07 ± 2.9E-09	1.09E-07 ± 3.0E-09	1.06E-07 ± 2.9E-09	1.09E-07 ± 3.0E-09	1.07E-07 ± 3.0E-09	1.06E-07 ± 2.9E-09
Fe	certified	7.49E-03 ± 1.6E-04	3.66E-03 ± 7.8E-05	3.64E-03 ± 7.8E-05	3.78E-03 ± 8.1E-05	3.67E-03 ± 7.8E-05	3.75E-03 ± 8.0E-05	3.69E-03 ± 7.9E-05	3.67E-03 ± 7.9E-05
H	certified	5.10E-02 ± 5E-04	2.49E-02 ± 2.5E-04	2.48E-02 ± 2.4E-04	2.57E-02 ± 2.5E-04	2.50E-02 ± 2.5E-04	2.55E-02 ± 2.5E-04	2.51E-02 ± 2.5E-04	2.50E-02 ± 2.5E-04
Hf	information	5E-07 ± NA	2.44E-07 ± NA	2.43E-07 ± NA	2.52E-07 ± NA	2.45E-07 ± NA	2.50E-07 ± NA	2.46E-07 ± NA	2.45E-07 ± NA
Hg	certified	9.28E-08 ± 3.3E-09	4.54E-08 ± 1.6E-09	4.51E-08 ± 1.6E-09	4.68E-08 ± 1.7E-09	4.54E-08 ± 1.6E-09	4.65E-08 ± 1.7E-09	4.57E-08 ± 1.6E-09	4.55E-08 ± 1.6E-09
K	certified	1.094E-03 ± 2.6E-05	5.35E-04 ± 1.3E-05	5.32E-04 ± 1.3E-05	5.52E-04 ± 1.3E-05	5.36E-04 ± 1.3E-05	5.48E-04 ± 1.3E-05	5.38E-04 ± 1.3E-05	5.37E-04 ± 1.3E-05
La	information	6E-06 ± NA	2.93E-06 ± NA	2.92E-06 ± NA	3.03E-06 ± NA	2.94E-06 ± NA	3.00E-06 ± NA	2.95E-06 ± NA	2.94E-06 ± NA
Mg	reference	3.90E-04 ± 6E-06	1.91E-04 ± 2.9E-06	1.90E-04 ± 2.9E-06	1.97E-04 ± 3.0E-06	1.91E-04 ± 2.9E-06	1.95E-04 ± 3.0E-06	1.92E-04 ± 3.0E-06	1.91E-04 ± 2.9E-06
Mn	reference	1.31E-05 ± 4E-07	6.40E-06 ± 2.0E-07	6.37E-06 ± 1.9E-07	6.61E-06 ± 2.0E-07	6.41E-06 ± 2.0E-07	6.56E-06 ± 2.0E-07	6.45E-06 ± 2.0E-07	6.43E-06 ± 2.0E-07
N	reference	1.59E-02 ± 1E-04	7.77E-03 ± 4.9E-05	7.73E-03 ± 4.9E-05	8.02E-03 ± 5.1E-05	7.78E-03 ± 5.0E-05	7.96E-03 ± 5.1E-05	7.83E-03 ± 5.0E-05	7.80E-03 ± 5.0E-05
Na	certified	2.969E-04 ± 4.2E-06	1.45E-04 ± 2.1E-06	1.44E-04 ± 2.0E-06	1.50E-04 ± 2.1E-06	1.45E-04 ± 2.1E-06	1.49E-04 ± 2.1E-06	1.46E-04 ± 2.1E-06	1.46E-04 ± 2.1E-06
Ni	information	1.0E-05 ± NA	4.89E-06 ± NA	4.86E-06 ± NA	5.04E-06 ± NA	4.90E-06 ± NA	5.01E-06 ± NA	4.92E-06 ± NA	4.90E-06 ± NA
Pb	certified	3.845E-06 ± 4.2E-08	1.88E-06 ± 2.1E-08	1.87E-06 ± 2.0E-08	1.94E-06 ± 2.1E-08	1.88E-06 ± 2.1E-08	1.92E-06 ± 2.1E-08	1.89E-06 ± 2.1E-08	1.89E-06 ± 2.1E-08
Rb	certified	7.36E-06 ± 2.0E-07	3.60E-06 ± 9.8E-08	3.58E-06 ± 9.7E-08	3.71E-06 ± 1.0E-07	3.60E-06 ± 9.8E-08	3.68E-06 ± 1.0E-07	3.62E-06 ± 9.8E-08	3.61E-06 ± 9.8E-08
S	certified	1.462E-02 ± 7.4E-04	7.15E-03 ± 3.6E-04	7.11E-03 ± 3.6E-04	7.38E-03 ± 3.7E-04	7.16E-03 ± 3.6E-04	7.32E-03 ± 3.7E-04	7.20E-03 ± 3.6E-04	7.17E-03 ± 3.6E-04
Sb	certified	4.45E-07 ± 1.5E-08	2.17E-07 ± 7.3E-09	2.16E-07 ± 7.3E-09	2.24E-07 ± 7.6E-09	2.18E-07 ± 7.3E-09	2.23E-07 ± 7.5E-09	2.19E-07 ± 7.4E-09	2.18E-07 ± 7.4E-09
Sc	reference	2.89E-06 ± 3E-08	1.41E-06 ± 1.5E-08	1.40E-06 ± 1.5E-08	1.46E-06 ± 1.5E-08	1.41E-06 ± 1.5E-08	1.45E-06 ± 1.5E-08	1.42E-06 ± 1.5E-08	1.42E-06 ± 1.5E-08
Se	reference	1.29E-06 ± 3E-08	6.30E-07 ± 1.5E-08	6.27E-07 ± 1.5E-08	6.51E-07 ± 1.5E-08	6.31E-07 ± 1.5E-08	6.46E-07 ± 1.5E-08	6.35E-07 ± 1.5E-08	6.33E-07 ± 1.5E-08
Si	reference	1.65E-02 ± 3E-04	8.06E-03 ± 1.5E-04	8.02E-03 ± 1.5E-04	8.32E-03 ± 1.5E-04	8.08E-03 ± 1.5E-04	8.26E-03 ± 1.5E-04	8.12E-03 ± 1.5E-04	8.09E-03 ± 1.5E-04
Sm	information	1E-06 ± NA	4.89E-07 ± NA	4.86E-07 ± NA	5.04E-07 ± NA	4.90E-07 ± NA	5.01E-07 ± NA	4.92E-07 ± NA	4.90E-07 ± NA
Sr	certified	6.35E-05 ± 1.2E-06	3.10E-05 ± 5.9E-07	3.09E-05 ± 5.8E-07	3.20E-05 ± 6.1E-07	3.11E-05 ± 5.9E-07	3.18E-05 ± 6.0E-07	3.13E-05 ± 5.9E-07	3.11E-05 ± 5.9E-07
Th	certified	1.428E-06 ± 3.5E-08	6.98E-07 ± 1.7E-08	6.94E-07 ± 1.7E-08	7.20E-07 ± 1.8E-08	6.99E-07 ± 1.7E-08	7.15E-07 ± 1.8E-08	7.03E-07 ± 1.7E-08	7.00E-07 ± 1.7E-08
Ti	certified	4.77E-04 ± 1.0E-05	2.33E-04 ± 4.9E-06	2.32E-04 ± 4.9E-06	2.41E-04 ± 5.1E-06	2.33E-04 ± 4.9E-06	2.39E-04 ± 5.0E-06	2.35E-04 ± 4.9E-06	2.34E-04 ± 4.9E-06
U	certified	5.17E-07 ± 1.2E-08	2.53E-07 ± 5.9E-09	2.51E-07 ± 5.8E-09	2.61E-07 ± 6.1E-09	2.53E-07 ± 5.9E-09	2.59E-07 ± 6.0E-09	2.54E-07 ± 5.9E-09	2.54E-07 ± 5.9E-09
V	certified	2.374E-05 ± 1.0E-07	1.16E-05 ± 5.0E-08	1.15E-05 ± 5.0E-08	1.20E-05 ± 5.2E-08	1.16E-05 ± 5.0E-08	1.19E-05 ± 5.1E-08	1.17E-05 ± 5.1E-08	1.16E-05 ± 5.0E-08
Zn	reference	1.29E-05 ± 1.2E-06	6.30E-06 ± 5.9E-07	6.27E-06 ± 5.8E-07	6.51E-06 ± 6.1E-07	6.31E-06 ± 5.9E-07	6.46E-06 ± 6.0E-07	6.35E-06 ± 5.9E-07	6.33E-06 ± 5.9E-07

Note: Listed values for mass fraction ± uncertainty were obtained from NIST SRM 1632d Certificate of Analysis (https://www-s.nist.gov/srmors/certificates/archives/1632d.pdf).
Note: Listed values for mass in sample ± uncertainty were calculated from mass fraction data and measured mass of dry powder added to each simulated sample.
Note: Elements studied in the round-robin test are highlighted yellow for QC-relevant impurities and blue for other tracked elements, including those of interest for PIE.

Table A-6. Impurity Content in SRM 1632d Added to Each ORNL Simulated Sample

NIST SRM1632d Data			ORNL-A	ORNL-B	ORNL-C	ORNL-D	ORNL-E	ORNL-F	ORNL-G
Mass of dried SRM1632d powder added (g):			0.5529 ± 0.0005	0.4850 ± 0.0005	0.5264 ± 0.0005	0.4922 ± 0.0005	0.4969 ± 0.0005	0.4904 ± 0.0005	0.4672 ± 0.0005
Element	Quality	SRM1632 mass fraction	Mass in sample (g)	Mass in sample (g)	Mass in sample (g)	Mass in sample (g)	Mass in sample (g)	Mass in sample (g)	Mass in sample (g)
Al	reference	9.12E-03 ± 5E-05	5.04E-03 ± 2.8E-05	4.42E-03 ± 2.5E-05	4.80E-03 ± 2.7E-05	4.49E-03 ± 2.5E-05	4.53E-03 ± 2.5E-05	4.47E-03 ± 2.5E-05	4.26E-03 ± 2.4E-05
As	reference	6.1E-06 ± 2E-07	3.37E-06 ± 1.1E-07	2.96E-06 ± 9.7E-08	3.21E-06 ± 1.1E-07	3.00E-06 ± 9.8E-08	3.03E-06 ± 9.9E-08	2.99E-06 ± 9.8E-08	2.85E-06 ± 9.3E-08
B	reference	6.2E-05 ± 1E-06	3.43E-05 ± 5.5E-07	3.01E-05 ± 4.9E-07	3.26E-05 ± 5.3E-07	3.05E-05 ± 4.9E-07	3.08E-05 ± 5.0E-07	3.04E-05 ± 4.9E-07	2.90E-05 ± 4.7E-07
Ba	certified	4.042E-05 ± 8.9E-07	2.23E-05 ± 4.9E-07	1.96E-05 ± 4.3E-07	2.13E-05 ± 4.7E-07	1.99E-05 ± 4.4E-07	2.01E-05 ± 4.4E-07	1.98E-05 ± 4.4E-07	1.89E-05 ± 4.2E-07
C	reference	7.688E-01 ± 1.5E-03	4.25E-01 ± 9.3E-04	3.73E-01 ± 8.2E-04	4.05E-01 ± 8.8E-04	3.78E-01 ± 8.3E-04	3.82E-01 ± 8.4E-04	3.77E-01 ± 8.3E-04	3.59E-01 ± 7.9E-04
Ca	reference	1.44E-03 ± 3E-05	7.96E-04 ± 1.7E-05	6.98E-04 ± 1.5E-05	7.58E-04 ± 1.6E-05	7.09E-04 ± 1.5E-05	7.15E-04 ± 1.5E-05	7.06E-04 ± 1.5E-05	6.73E-04 ± 1.4E-05
Cd	reference	8E-08 ± 1E-08	4.42E-08 ± 5.5E-09	3.88E-08 ± 4.9E-09	4.21E-08 ± 5.3E-09	3.94E-08 ± 4.9E-09	3.97E-08 ± 5.0E-09	3.92E-08 ± 4.9E-09	3.74E-08 ± 4.7E-09
Ce	reference	1.17E-05 ± 4E-07	6.47E-06 ± 2.2E-07	5.67E-06 ± 1.9E-07	6.16E-06 ± 2.1E-07	5.76E-06 ± 2.0E-07	5.81E-06 ± 2.0E-07	5.74E-06 ± 2.0E-07	5.47E-06 ± 1.9E-07
Cl	certified	1.142E-03 ± 1.1E-05	6.31E-04 ± 6.1E-06	5.54E-04 ± 5.4E-06	6.01E-04 ± 5.8E-06	5.62E-04 ± 5.4E-06	5.67E-04 ± 5.5E-06	5.60E-04 ± 5.4E-06	5.34E-04 ± 5.2E-06
Co	certified	3.424E-06 ± 4.8E-08	1.89E-06 ± 2.7E-08	1.66E-06 ± 2.3E-08	1.80E-06 ± 2.5E-08	1.69E-06 ± 2.4E-08	1.70E-06 ± 2.4E-08	1.68E-06 ± 2.4E-08	1.60E-06 ± 2.2E-08
Cr	reference	1.37E-05 ± 1E-07	7.57E-06 ± 5.6E-08	6.64E-06 ± 4.9E-08	7.21E-06 ± 5.3E-08	6.74E-06 ± 5.0E-08	6.81E-06 ± 5.0E-08	6.72E-06 ± 4.9E-08	6.40E-06 ± 4.7E-08
Cs	reference	5.98E-07 ± 6E-09	3.31E-07 ± 3.3E-09	2.90E-07 ± 2.9E-09	3.15E-07 ± 3.2E-09	2.94E-07 ± 3.0E-09	2.97E-07 ± 3.0E-09	2.93E-07 ± 3.0E-09	2.79E-07 ± 2.8E-09
Cu	certified	5.83E-06 ± 3.1E-07	3.22E-06 ± 1.7E-07	2.83E-06 ± 1.5E-07	3.07E-06 ± 1.6E-07	2.87E-06 ± 1.5E-07	2.90E-06 ± 1.5E-07	2.86E-06 ± 1.5E-07	2.72E-06 ± 1.4E-07
Dy	information	9E-07 ± NA	4.98E-07 ± NA	4.37E-07 ± NA	4.74E-07 ± NA	4.43E-07 ± NA	4.47E-07 ± NA	4.41E-07 ± NA	4.20E-07 ± NA
Eu	reference	2.17E-07 ± 6E-09	1.20E-07 ± 3.3E-09	1.05E-07 ± 2.9E-09	1.14E-07 ± 3.2E-09	1.07E-07 ± 3.0E-09	1.08E-07 ± 3.0E-09	1.06E-07 ± 2.9E-09	1.01E-07 ± 2.8E-09
Fe	certified	7.49E-03 ± 1.6E-04	4.14E-03 ± 8.9E-05	3.63E-03 ± 7.8E-05	3.94E-03 ± 8.4E-05	3.69E-03 ± 7.9E-05	3.72E-03 ± 8.0E-05	3.67E-03 ± 7.9E-05	3.50E-03 ± 7.5E-05
H	certified	5.10E-02 ± 5E-04	2.82E-02 ± 2.8E-04	2.47E-02 ± 2.4E-04	2.68E-02 ± 2.6E-04	2.51E-02 ± 2.5E-04	2.53E-02 ± 2.5E-04	2.50E-02 ± 2.5E-04	2.38E-02 ± 2.3E-04
Hf	information	5E-07 ± NA	2.76E-07 ± NA	2.43E-07 ± NA	2.63E-07 ± NA	2.46E-07 ± NA	2.48E-07 ± NA	2.45E-07 ± NA	2.34E-07 ± NA
Hg	certified	9.28E-08 ± 3.3E-09	5.13E-08 ± 1.8E-09	4.50E-08 ± 1.6E-09	4.89E-08 ± 1.7E-09	4.57E-08 ± 1.6E-09	4.61E-08 ± 1.6E-09	4.55E-08 ± 1.6E-09	4.34E-08 ± 1.5E-09
K	certified	1.094E-03 ± 2.6E-05	6.05E-04 ± 1.4E-05	5.31E-04 ± 1.3E-05	5.76E-04 ± 1.4E-05	5.39E-04 ± 1.3E-05	5.44E-04 ± 1.3E-05	5.36E-04 ± 1.3E-05	5.11E-04 ± 1.2E-05
La	information	6E-06 ± NA	3.32E-06 ± NA	2.91E-06 ± NA	3.16E-06 ± NA	2.95E-06 ± NA	2.98E-06 ± NA	2.94E-06 ± NA	2.80E-06 ± NA
Mg	reference	3.90E-04 ± 6E-06	2.16E-04 ± 3.3E-06	1.89E-04 ± 2.9E-06	2.05E-04 ± 3.2E-06	1.92E-04 ± 3.0E-06	1.94E-04 ± 3.0E-06	1.91E-04 ± 2.9E-06	1.82E-04 ± 2.8E-06
Mn	reference	1.31E-05 ± 4E-07	7.24E-06 ± 2.2E-07	6.35E-06 ± 1.9E-07	6.90E-06 ± 2.1E-07	6.45E-06 ± 2.0E-07	6.51E-06 ± 2.0E-07	6.42E-06 ± 2.0E-07	6.12E-06 ± 1.9E-07
N	reference	1.59E-02 ± 1E-04	8.79E-03 ± 5.6E-05	7.71E-03 ± 4.9E-05	8.37E-03 ± 5.3E-05	7.83E-03 ± 5.0E-05	7.90E-03 ± 5.0E-05	7.80E-03 ± 5.0E-05	7.43E-03 ± 4.7E-05
Na	certified	2.969E-04 ± 4.2E-06	1.64E-04 ± 2.3E-06	1.44E-04 ± 2.0E-06	1.56E-04 ± 2.2E-06	1.46E-04 ± 2.1E-06	1.48E-04 ± 2.1E-06	1.46E-04 ± 2.1E-06	1.39E-04 ± 2.0E-06
Ni	information	1.0E-05 ± NA	5.53E-06 ± NA	4.85E-06 ± NA	5.26E-06 ± NA	4.92E-06 ± NA	4.97E-06 ± NA	4.90E-06 ± NA	4.67E-06 ± NA
Pb	certified	3.845E-06 ± 4.2E-08	2.13E-06 ± 2.3E-08	1.86E-06 ± 2.0E-08	2.02E-06 ± 2.2E-08	1.89E-06 ± 2.1E-08	1.91E-06 ± 2.1E-08	1.89E-06 ± 2.1E-08	1.80E-06 ± 2.0E-08
Rb	certified	7.36E-06 ± 2.0E-07	4.07E-06 ± 1.1E-07	3.57E-06 ± 9.7E-08	3.87E-06 ± 1.1E-07	3.62E-06 ± 9.9E-08	3.66E-06 ± 9.9E-08	3.61E-06 ± 9.8E-08	3.44E-06 ± 9.4E-08
S	certified	1.462E-02 ± 7.4E-04	8.08E-03 ± 4.1E-04	7.09E-03 ± 3.6E-04	7.70E-03 ± 3.9E-04	7.20E-03 ± 3.6E-04	7.26E-03 ± 3.7E-04	7.17E-03 ± 3.6E-04	6.83E-03 ± 3.5E-04
Sb	certified	4.45E-07 ± 1.5E-08	2.46E-07 ± 8.3E-09	2.16E-07 ± 7.3E-09	2.34E-07 ± 7.9E-09	2.19E-07 ± 7.4E-09	2.21E-07 ± 7.5E-09	2.18E-07 ± 7.4E-09	2.08E-07 ± 7.0E-09
Sc	reference	2.89E-06 ± 3E-08	1.60E-06 ± 1.7E-08	1.40E-06 ± 1.5E-08	1.52E-06 ± 1.6E-08	1.42E-06 ± 1.5E-08	1.44E-06 ± 1.5E-08	1.42E-06 ± 1.5E-08	1.35E-06 ± 1.4E-08
Se	reference	1.29E-06 ± 3E-08	7.13E-07 ± 1.7E-08	6.26E-07 ± 1.5E-08	6.79E-07 ± 1.6E-08	6.35E-07 ± 1.5E-08	6.41E-07 ± 1.5E-08	6.33E-07 ± 1.5E-08	6.03E-07 ± 1.4E-08
Si	reference	1.65E-02 ± 3E-04	9.12E-03 ± 1.7E-04	8.00E-03 ± 1.5E-04	8.69E-03 ± 1.6E-04	8.12E-03 ± 1.5E-04	8.20E-03 ± 1.5E-04	8.09E-03 ± 1.5E-04	7.71E-03 ± 1.4E-04
Sm	information	1E-06 ± NA	5.53E-07 ± NA	4.85E-07 ± NA	5.26E-07 ± NA	4.92E-07 ± NA	4.97E-07 ± NA	4.90E-07 ± NA	4.67E-07 ± NA
Sr	certified	6.35E-05 ± 1.2E-06	3.51E-05 ± 6.6E-07	3.08E-05 ± 5.8E-07	3.34E-05 ± 6.3E-07	3.13E-05 ± 5.9E-07	3.16E-05 ± 6.0E-07	3.11E-05 ± 5.9E-07	2.97E-05 ± 5.6E-07
Th	certified	1.428E-06 ± 3.5E-08	7.89E-07 ± 1.9E-08	6.93E-07 ± 1.7E-08	7.52E-07 ± 1.8E-08	7.03E-07 ± 1.7E-08	7.10E-07 ± 1.7E-08	7.00E-07 ± 1.7E-08	6.67E-07 ± 1.6E-08
Ti	certified	4.77E-04 ± 1.0E-05	2.64E-04 ± 5.5E-06	2.31E-04 ± 4.9E-06	2.51E-04 ± 5.3E-06	2.35E-04 ± 4.9E-06	2.37E-04 ± 5.0E-06	2.34E-04 ± 4.9E-06	2.23E-04 ± 4.7E-06
U	certified	5.17E-07 ± 1.2E-08	2.86E-07 ± 6.6E-09	2.51E-07 ± 5.8E-09	2.72E-07 ± 6.3E-09	2.54E-07 ± 5.9E-09	2.57E-07 ± 6.0E-09	2.54E-07 ± 5.9E-09	2.42E-07 ± 5.6E-09
V	certified	2.374E-05 ± 1.0E-07	1.31E-05 ± 5.7E-08	1.15E-05 ± 5.0E-08	1.25E-05 ± 5.4E-08	1.17E-05 ± 5.1E-08	1.18E-05 ± 5.1E-08	1.16E-05 ± 5.0E-08	1.11E-05 ± 4.8E-08
Zn	reference	1.29E-05 ± 1.2E-06	7.13E-06 ± 6.6E-07	6.26E-06 ± 5.8E-07	6.79E-06 ± 6.3E-07	6.35E-06 ± 5.9E-07	6.41E-06 ± 6.0E-07	6.33E-06 ± 5.9E-07	6.03E-06 ± 5.6E-07

Note: Listed values for mass fraction ± uncertainty were obtained from NIST SRM 1632d Certificate of Analysis (https://www-s.nist.gov/srmors/certificates/archives/1632d.pdf).
Note: Listed values for mass in sample ± uncertainty were calculated from mass fraction data and measured mass of dry powder added to each simulated sample.
Note: Elements studied in the round-robin test are highlighted yellow for QC-relevant impurities and blue for other tracked elements, including those of interest for PIE.